



# On the dynamic behaviour of rotating shafts under combined axial and torsional loads

Alessandro De Felice · Silvio Sorrentino

Received: 10 December 2018 / Accepted: 25 April 2019 / Published online: 20 May 2019  
© Springer Nature B.V. 2019

**Abstract** A comprehensive dynamic study on a distributed parameter model of a straight uniform rotating shaft is developed, aimed at presenting some clarifications and corrections to published results, together with novel contributions. The model includes the effects of transverse shear, rotatory inertia and gyroscopic moments with additional combined end thrust and twisting moment. The equations of motion are derived in both Newtonian and Lagrangian formulations according to the Timoshenko beam theory. A novel contribution is given in the development of complete modal analysis of the model under study, highlighting the properties of the operators involved and the relations among eigenfunctions represented in complex and real variables. The influence of the main governing parameters (slenderness ratio, angular velocity, external axial end thrust and twisting moment) is studied on natural frequencies, modal shapes and critical speeds of the rotor. New evidence of existence of a second frequency spectrum in the Timoshenko beam theory is presented, together with a novel definition for its identification, only possible if considering gyroscopic effects.

**Keywords** Rotating shaft · Timoshenko beam · Gyroscopic moment · Axial end thrust · Twisting moment · Second spectrum

## 1 Introduction

The general increasing trend towards high speed rotating equipment in conjunction with higher power density encourages further insights into the understanding of the dynamic behaviour of torque-transmitting flexible rotors. In this research field the use of finite element models is nowadays widespread, however distributed parameter formulations still remain of some interest, at least for analytical investigations and validation purposes.

Continuous models of rotating shafts have been studied by several researchers who have dealt with many important aspects, highlighting the effects of transverse shear, rotatory inertia, gyroscopic moments and considering the additional contribution of axial end thrust and twisting moment.

The gyroscopic effects were studied considering rotating Timoshenko beams. The equilibrium equations for symmetric and asymmetric rotors, without the contribution of axial loads, were derived by Dimentberg [1] adopting the Newtonian formulation and later by Raffa and Vatta [2, 3] with Lagrangian formulation via Hamilton's principle, while the case of

---

A. De Felice · S. Sorrentino (✉)  
Department of Engineering Enzo Ferrari, University of  
Modena and Reggio Emilia, Via Pietro Vivarelli 10,  
41125 Modena, Italy  
e-mail: silvio.sorrentino@unimore.it

eccentric rotation was studied by Filipich and Rosales [4].

Early investigations about the effects of axial end thrust and twisting moment of constant magnitude acting simultaneously on a uniform shaft can be found in the works of Greenhill [5] and Southwell and Gough [6], who first considered the influence of these loads on critical speeds.

More recently, the effects of an axial end twisting moment alone on the flexural behaviour of a rotating slender shaft was studied according to the Euler–Bernoulli beam model by Colomb and Rosenberg [7], and according to the Timoshenko beam model by Eshleman and Eubanks [8], who focused their analysis on critical speeds without considering natural frequencies. They found that the Euler–Bernoulli model is inaccurate in predicting the critical speeds, and that the latter always decrease with external axial torque. Following the results by Eshleman and Eubanks, the topic was then again considered, among others, by Yim et al. [9].

The equations of motion of a rotating Timoshenko beam subjected to axial end thrust were derived with Lagrangian formulation by Choi et al. [10]. An analysis of the effects of combined external axial end thrust and twisting moment was proposed by Willems and Holzer [11] and later by Dubigeon and Michon [12], who adopted the Timoshenko beam model, casting doubts on some results obtained by Eshleman and Eubanks. It should also be remarked that while most authors studied natural frequencies and critical speeds, only a few of them developed a complete modal analysis of a distributed parameter rotating shaft, as for instance Lee et al. [13] in the case of a rotating Rayleigh beam.

In this study further insights are proposed in the analysis of a distributed parameter model of a high-speed, power transmitting flexible rotor. A homogeneous uniform Timoshenko straight beam with circular section is considered, rotating with constant angular speed about its longitudinal axis on isotropic supports (rigid bearings), and subjected simultaneously to constant end thrust and twisting moment. The equations of motion differ from those derived in [12], and are consistent with those obtained in less general cases [8, 10]. A novel contribution is given in the development of complete modal analysis of the model under study, clarifying the properties of the operators involved and the relations among eigenfunctions

represented in complex and real variables. In addition, such analytical developments allow to cast new light on the problem of existence and identification of the second frequency spectrum in the Timoshenko beam theory [14], here reconsidered from a novel perspective. The existence of a second spectrum in the case of non-rotating beams and general boundary conditions has been much debated in the literature [15–17], since it is possible to easily identify the companion natural frequencies constituting the second spectrum only in particular cases. More recently, the existence of a second spectrum in a non-rotating finite-length beam has been demonstrated on the basis of accurate experimental results, at least for free–free boundary conditions [18], and also by considering free waves in beams of infinite length [19]. In this study new evidence of existence of the second spectrum together with a novel definition for its identification are presented, only possible if considering gyroscopic effects, therefore a rotating beam. In parallel, the role of the so-called cut-off Timoshenko beam frequencies [16] is investigated, extending their definition to include the effects of gyroscopic moments and external loads [20, 21].

The article is organized as follows: in Sect. 2, the equations of motion of the rotating shaft are derived under the small strain assumption in both Newtonian and Lagrangian formulations, and represented in a state-space operator form; in Sect. 3, the equations of motion are decoupled using both real and complex displacement variables, and then cast in nondimensional form to facilitate the analysis of the effects of each governing parameter; the general integral is sought by following a complex-variable approach, yielding eigenfrequencies, closed-form expressions of the eigenfunctions, and critical speeds; in Sect. 4, modal analysis of the rotating shaft is completed for real displacement variables in both the configuration space and in the state-space, including the derivation of critical loads due to combined effects of axial end thrust and twisting moment; in Sect. 5, a systematic study of the influence of slenderness ratio, angular speed, axial end thrust and twisting moment is conducted to determine their relative importance on natural frequencies, mode shapes and critical speeds; on the basis of the results presented in the previous section, a novel criterion is given and discussed for the definition and identification of the second frequency spectrum in the Timoshenko beam theory.

## 2 Equations of motion

After a brief description of the rotating shaft model, its equations of motion are derived adopting the small strain assumption [10] in both Newtonian and Lagrangian formulations, and finally represented in a state-space operator form.

### 2.1 Model description and nomenclature

A homogeneous uniform Timoshenko straight beam with circular section is considered, rotating at constant angular speed about its longitudinal axis and simultaneously subjected to axial end thrust and twisting moment. The model is characterized by the following parameters:

$A = \pi r^2 =$ cross-sectional area [m <sup>2</sup> ]	$\kappa =$ transverse shear factor
$l =$ length of the shaft [m]	$N =$ axial end thrust [N]
$E =$ Young's modulus [N/m <sup>2</sup> ]	$T =$ axial end twisting moment [Nm]
$G =$ shear elasticity modulus [N/m <sup>2</sup> ]	$\nu =$ Poisson's ratio
$I_y = I_z = J =$ moment of inertia of the cross-section [m <sup>4</sup> ]	$\rho =$ density [Kg/m <sup>3</sup> ]
$I_x = 2J =$ polar moment of inertia of the cross-section [m <sup>4</sup> ]	$\omega =$ rotating angular speed [rad/s]

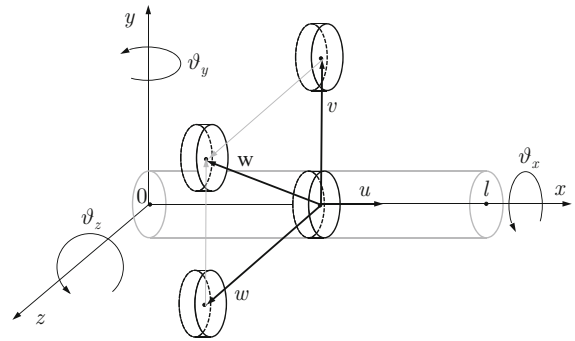


**Fig. 1** Schematic representation of displacements

The external loads  $N$  (positive if tensile) and  $T$  (positive if counterclockwise) are assumed constant with respect to time. Isotropic supports are considered, making the whole model axisymmetric. Hence it can be represented in a non-rotating coordinate system as shown in Fig. 1. Additional nomenclature includes:

- $u, v, w =$  displacements in the  $x, y, z$  directions, respectively [m]
- $w = v + iw =$  complex displacement [m]
- $\vartheta_x, \vartheta_y, \vartheta_z =$  angular displacements about the  $x, y, z$  axes, respectively [rad]
- $\theta = \vartheta_y + i\vartheta_z =$  complex angular displacement [rad]

In next sections a simplified notation for partial derivatives is adopted, dots denoting differentiation with respect to time and roman numbers denoting differentiation with respect to the spatial coordinate  $x$ .

### 2.2 Newtonian formulation of the equations of motion

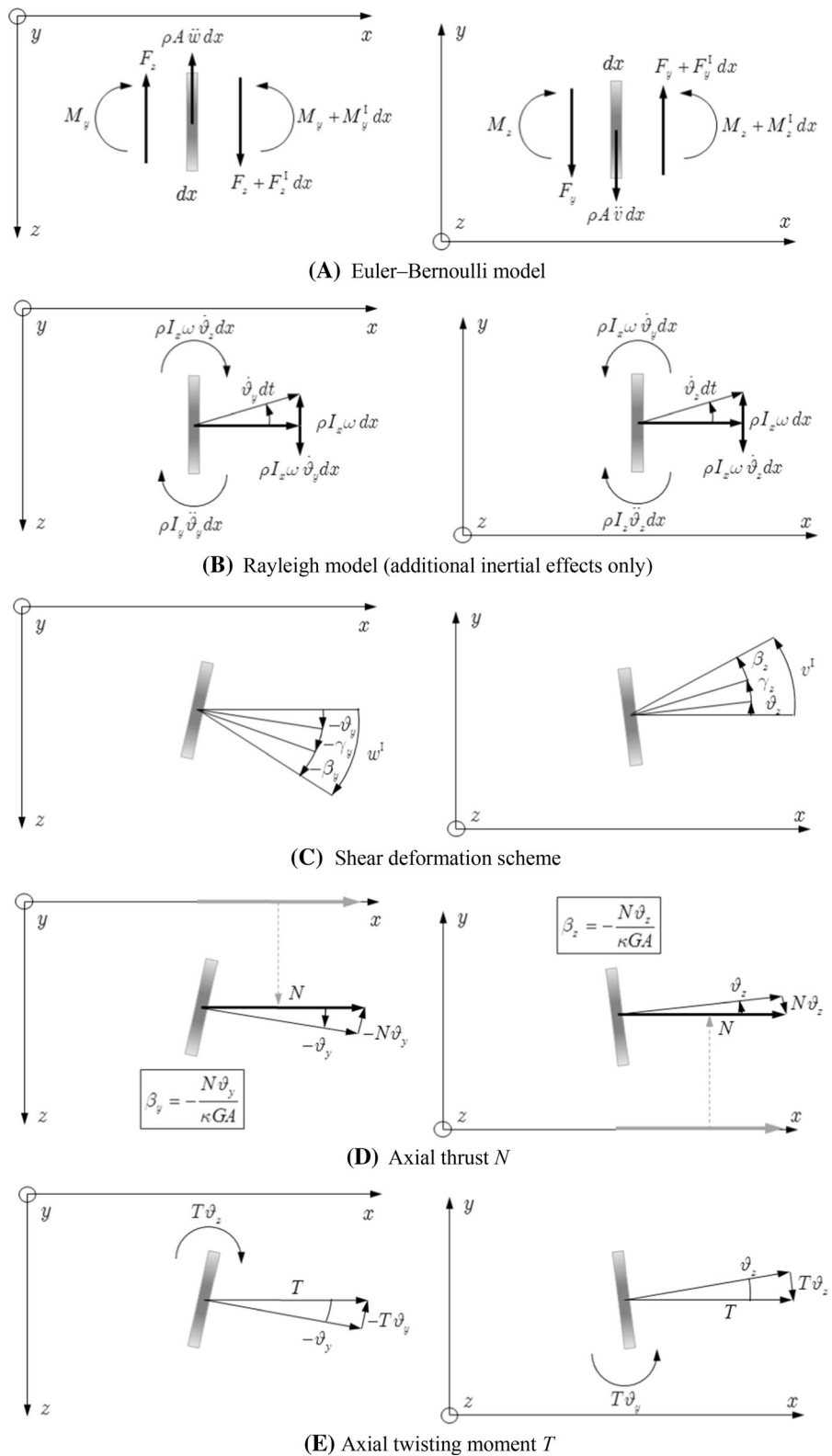
The linear equations of motion of the loaded rotating shaft are obtained with Newtonian formulation, referring to the nomenclature introduced in Sect. 2.1 and to the equilibrium schemes for a section of infinitesimal length  $dx$  reported in Fig. 2.

The  $x$ -direction translational and rotational well-known equations of motion are decoupled:

$$\begin{cases} F_x + [H(x) - H(x - l)] N = EA u^I \\ F_x^I = \rho A \ddot{u} \\ M_x + [H(x) - H(x - l)] T = 2GJ \vartheta_x^I \\ M_x^I = 2\rho J \ddot{\vartheta}_x \end{cases}, \tag{1}$$

where  $H(\cdot)$  represents the Heaviside unit step distribution. The equation of motion describing the flexural behaviour in the  $x$ - $y$  plane can be written starting from the expression of the shear angle  $\gamma_z$  (caused by the

**Fig. 2** Equilibrium schemes for a cross-section of infinitesimal length  $dx$



shear force  $F_y$ ) in terms of  $\vartheta_z, v^I$  and of the shear angle  $\beta_z$  (caused by the external action  $N$ ), according to the schemes reported in Fig. 2C and D, right side:

$$\vartheta_z + \gamma_z + \beta_z = v^I, \quad \begin{cases} \gamma_z = \frac{F_y}{\kappa GA} \\ \beta_z = -\frac{N\vartheta_z}{\kappa GA} \end{cases} \Rightarrow \vartheta_z = \frac{1}{\psi} \left( v^I - \frac{F_y}{\kappa GA} \right), \quad \psi = 1 - \frac{N}{\kappa GA} \quad (2)$$

The constitutive equation for  $F_y$  given by Eq. (2) together with the  $y$ -direction translational dynamic equilibrium (Fig. 2A, right side) yield the following differential link between  $\vartheta_z$  and  $v$ :

$$\begin{cases} F_y = \kappa GA (v^I - \psi \vartheta_z) \\ F_y^I = \rho A \ddot{v} \end{cases} \Rightarrow \vartheta_z^I = \frac{1}{\psi} \left( v^{II} - \frac{\rho}{\kappa G} \ddot{v} \right) \quad (3)$$

Taking into account the effects of  $N$  and  $T$  in the constitutive equation for the bending moment  $M_z$  (Fig. 2D and E, right side) together with the rotational dynamic equilibrium in the  $x$ - $y$  plane (Fig. 2A, right side) gives:

$$\begin{cases} M_z + T\vartheta_y + Nv = EJ\vartheta_z^I \\ M_z^I + F_y = \rho J\ddot{\vartheta}_z - 2\rho J\omega\dot{\vartheta}_y \end{cases} \Rightarrow EJ\vartheta_z^{II} - T\vartheta_y^I - Nv^I + F_y = \rho J\ddot{\vartheta}_z - 2\rho J\omega\dot{\vartheta}_y \quad (4)$$

Finally, differentiating Eq. (4) and introducing the expression of  $F_y$  given by Eq. (3) leads to the equation of motion in the form:

$$EJ\vartheta_z^{III} - T\vartheta_y^{II} - Nv^{II} + \rho A \ddot{v} - \rho J\ddot{\vartheta}_z^I + 2\rho J\omega\dot{\vartheta}_y^I = 0 \quad (5)$$

The equation of motion describing the flexural behaviour in the  $x$ - $z$  plane can be written following the same steps, paying attention to sign conventions (Fig. 2A–E, left side):

$$EJ\vartheta_y^{III} + T\vartheta_z^{II} + Nw^{II} - \rho A \ddot{w} - \rho J\ddot{\vartheta}_y^I - 2\rho J\omega\dot{\vartheta}_z^I = 0 \quad (6)$$

The flexural degrees of freedom in the  $x$ - $y$  and  $x$ - $z$  planes are coupled due to both gyroscopic and axial twisting moments. Distributed external loads along the

$x$  coordinate could be considered introducing non-homogeneous terms in Eqs. (5) and (6).

### 2.3 Lagrangian formulation of the equations of motion

The same linear equations of motion of the loaded rotating shaft are obtained by applying Hamilton’s principle to a Lagrangian density function  $\mathcal{L} = \mathcal{T} - \mathcal{V} + \mathcal{W}$ , written in terms of kinetic energy density  $\mathcal{T}$ , potential energy density  $\mathcal{V}$  and associating a work density  $\mathcal{W}$  to the external loads, which are not derivable from a potential. Referring to the nomenclature introduced in Sect. 2.1, the kinetic energy density takes the form:

$$\mathcal{T} = \frac{1}{2} \rho \left[ A (\dot{u}^2 + \dot{v}^2 + \dot{w}^2) + J(2\dot{\vartheta}_x^2 + \dot{\vartheta}_y^2 + \dot{\vartheta}_z^2) + 2J\omega^2 + 4J\omega\dot{\vartheta}_x + 2J\omega(\vartheta_z\dot{\vartheta}_y - \vartheta_y\dot{\vartheta}_z) \right] \quad (7)$$

which is derived in “Appendix A” (following an alternative method with respect to standard formulations), while according to [2, 10, 22] the potential energy density reads:

$$\mathcal{V} = \frac{1}{2} \left\{ EA (u^I)^2 + EJ \left[ (\vartheta_y^I)^2 + (\vartheta_z^I)^2 \right] + \kappa GA \left[ (-w^I - \vartheta_y)^2 + (v^I - \vartheta_z)^2 \right] + 2JG(\vartheta_x^I)^2 \right\} \quad (8)$$

The inclusion of external loads  $N$  and  $T$  in the rotating Timoshenko beam model is debated in the literature, leading to different forms of the equations

of motion [8, 10, 12, 22]. Here the following expression of the work density is adopted:

$$\mathcal{W} = \frac{1}{2} \left\{ T(\vartheta_y \vartheta_z^I - \vartheta_y^I \vartheta_z) - N \left[ (v^I)^2 - (v^I - \vartheta_z)^2 + (w^I)^2 - (-w^I - \vartheta_y)^2 \right] \right\} + [\delta(x-l) - \delta(x)] [Nu + T\vartheta_x] \tag{9}$$

where  $\delta(\cdot)$  represents the Dirac distribution. In Eq. (9), the first term (related to  $T$ ) can be immediately obtained referring to the schemes reported in Fig. 2D, noticing that its expression is not unique (due to symmetry), in the sense that it could be written in a more general form as:

$$\mathcal{W}_T = T(c_1 \vartheta_y \vartheta_z^I - c_2 \vartheta_y^I \vartheta_z), \tag{10}$$

$$c_1 \in [0, 1], \quad c_2 = 1 - c_1$$

leading in any case to the same equations of motion. Similar remarks also apply to the gyroscopic terms in the kinetic energy density, Eq. (7), as explained in detail in [2].

The second term in Eq. (9) (related to  $N$ ) is derived according with [10] taking into account the axial geometric shortening of the shaft, which ensures consistency with the Timoshenko beam model. Introducing Eqs. (7)–(9) in Lagrange’s equations for a continuous second-order one-dimensional problem:

$$\frac{\partial}{\partial t} \left( \frac{\partial \mathcal{L}}{\partial \dot{q}_t} \right) + \frac{\partial}{\partial x} \left( \frac{\partial \mathcal{L}}{\partial q_t^I} \right) - \frac{\partial \mathcal{L}}{\partial q_t} = 0, \tag{11}$$

$$\mathbf{q}_t = \{u, v, w, \vartheta_x, \vartheta_y, \vartheta_z\}^T$$

yields the following six equations of motion:

The first and fourth of Eq. (12) are decoupled, representing the  $x$ -direction translational and rotational dynamic equilibrium equations respectively. The other four equations, representing the flexural dynamic equilibrium of the shaft, are rewritten in a more compact form introducing the parameter  $\psi$ , defined as a function of  $N$  in Eq. (2):

$$\begin{cases} \rho A \ddot{v} - \kappa GA (v^{II} - \psi \vartheta_z^I) = 0 \\ \rho A \ddot{w} - \kappa GA (w^{II} + \psi \vartheta_y^I) = 0 \\ \rho J \ddot{\vartheta}_y + 2\rho J \omega \dot{\vartheta}_z + \kappa GA \psi (w^I + \vartheta_y) - EJ \vartheta_y^{II} - T \vartheta_z^I = 0 \\ \rho J \ddot{\vartheta}_z - 2\rho J \omega \dot{\vartheta}_y - \kappa GA \psi (v^I - \vartheta_z) - EJ \vartheta_z^{II} + T \vartheta_y^I = 0 \end{cases} \tag{13}$$

The first of Eq. (13) yields the differential link between  $\vartheta_z$  and  $v$  already given in Eq. (3), while the second one provides the analogous relation between  $\vartheta_y$  and  $w$ . Introducing them into the last two of Eq. (13) gives the equations of motion in the form of Eqs. (5) and (6).

### 2.4 Operator form of the equations of motion

Equations (13) can also be expressed in operator form, as a function of a vector  $\mathbf{q}$  defined in the configuration space by the four flexural lagrangian coordinates:

$$\mathbf{M} \ddot{\mathbf{q}} + \mathbf{G} \dot{\mathbf{q}} + [\mathcal{K}] \mathbf{q} = \mathbf{0}, \quad \mathbf{q} = \{v, w, \vartheta_y, \vartheta_z\}^T \tag{14}$$

where  $\mathbf{M}$  and  $\mathbf{G}$  are linear algebraic operators, diagonal and skew-symmetric respectively:

$$\begin{cases} \rho A \ddot{u} - EA u^{II} - [\delta(x-l) - \delta(x)] N = 0 \\ \rho A \ddot{v} - \kappa GA (v^{II} - \vartheta_z^I) - N \vartheta_z^I = 0 \\ \rho A \ddot{w} - \kappa GA (w^{II} + \vartheta_y^I) + N \vartheta_y^I = 0 \\ 2\rho J \ddot{\vartheta}_x - 2GJ \vartheta_x^{II} - [\delta(x-l) - \delta(x)] T = 0 \\ \rho J \ddot{\vartheta}_y + 2\rho J \omega \dot{\vartheta}_z + \kappa GA (w^I + \vartheta_y) - EJ \vartheta_y^{II} - T \vartheta_z^I - N (w^I + \vartheta_y) = 0 \\ \rho J \ddot{\vartheta}_z - 2\rho J \omega \dot{\vartheta}_y - \kappa GA (v^I - \vartheta_z) - EJ \vartheta_z^{II} + T \vartheta_y^I + N (v^I - \vartheta_z) = 0 \end{cases} \tag{12}$$

$$\mathbf{M} = \begin{bmatrix} \rho A & 0 & 0 & 0 \\ 0 & \rho A & 0 & 0 \\ 0 & 0 & \rho J & 0 \\ 0 & 0 & 0 & \rho J \end{bmatrix}, \tag{15}$$

$$\mathbf{G} = \begin{bmatrix} 0 & 0 & 0 & 0 \\ 0 & 0 & 0 & 0 \\ 0 & 0 & 0 & 2\rho J\omega \\ 0 & 0 & -2\rho J\omega & 0 \end{bmatrix}$$

and  $[\mathcal{K}(\cdot)]$  is a linear second order differential

$$[\mathcal{K}(\cdot)] = \begin{bmatrix} -\kappa GA (\cdot)^{\text{II}} & 0 & 0 & \kappa GA \psi (\cdot)^{\text{I}} \\ 0 & -\kappa GA (\cdot)^{\text{II}} & -\kappa GA \psi (\cdot)^{\text{I}} & 0 \\ 0 & \kappa GA \psi (\cdot)^{\text{I}} & \kappa GA \psi (\cdot) - EJ (\cdot)^{\text{II}} & -T (\cdot)^{\text{I}} \\ -\kappa GA \psi (\cdot)^{\text{I}} & 0 & T (\cdot)^{\text{I}} & \kappa GA \psi (\cdot) - EJ (\cdot)^{\text{II}} \end{bmatrix} \tag{16}$$

Hence the adjoint operators of the matrices  $\mathbf{M}$ ,  $\mathbf{G}$ ,  $\mathbf{A}$  and of the differential operators  $[\mathcal{K}(\cdot)]$  and  $[\mathcal{B}(\cdot)]$ , assuming same boundary conditions at both ends of the shaft, are simply:

$$\tilde{\mathbf{M}} = \mathbf{M}, \quad \tilde{\mathbf{G}} = \mathbf{G}^T, \quad \tilde{\mathbf{A}} = \mathbf{A}^T, \tag{19}$$

$$[\tilde{\mathcal{K}}(\cdot)] = [\mathcal{K}(\cdot)]^T, \quad [\tilde{\mathcal{B}}(\cdot)] = [\mathcal{B}(\cdot)]^T$$

due to skew-symmetry (and first-order derivatives in differential operators) of all terms out of their main diagonals.

operator, non-self-adjoint:

A possible state-space representation of Eq. (14), as a function of a vector  $\mathbf{q}_s$ , reads:

$$\mathbf{A} \dot{\mathbf{q}}_s + [\mathcal{B}] \mathbf{q}_s = \mathbf{0}, \quad \mathbf{q}_s = \{ \mathbf{q}^T, \dot{\mathbf{q}}^T \}^T, \tag{17}$$

$$\mathbf{A} = \begin{bmatrix} \mathbf{G} & \mathbf{M} \\ -\mathbf{M} & \mathbf{0} \end{bmatrix}, \quad [\mathcal{B}(\cdot)] = \begin{bmatrix} [\mathcal{K}(\cdot)] & \mathbf{0} \\ \mathbf{0} & \mathbf{M} \end{bmatrix}$$

where  $\mathbf{A}$  is a linear algebraic operator, skew-symmetric, and  $[\mathcal{B}(\cdot)]$  is a linear second order differential operator, non-self-adjoint.

Considering two different functions, say  $\Phi_h$  and  $\Phi_k$ , the general definition of the adjoint form of an operator  $[\mathcal{O}(\cdot)]$ , denoted by the tilde symbol, is given by the following inner products [13]:

$$\begin{cases} EJ \left( v^{\text{IV}} - \frac{\rho}{\kappa G} \dot{v}^{\text{II}} \right) + T \left( w^{\text{III}} - \frac{\rho}{\kappa G} \dot{w}^{\text{I}} \right) - N \psi v^{\text{II}} + \rho A \psi \ddot{v} - \rho J \left( \ddot{v}^{\text{II}} - \frac{\rho}{\kappa G} \ddot{\dot{v}} \right) - 2\rho J\omega \left( \dot{w}^{\text{II}} - \frac{\rho}{\kappa G} \ddot{w} \right) = 0 \\ EJ \left( w^{\text{IV}} - \frac{\rho}{\kappa G} \dot{w}^{\text{II}} \right) - T \left( v^{\text{III}} - \frac{\rho}{\kappa G} \dot{v}^{\text{I}} \right) - N \psi w^{\text{II}} + \rho A \psi \ddot{w} - \rho J \left( \ddot{w}^{\text{II}} - \frac{\rho}{\kappa G} \ddot{\dot{w}} \right) + 2\rho J\omega \left( \dot{v}^{\text{II}} - \frac{\rho}{\kappa G} \ddot{v} \right) = 0 \end{cases} \tag{20}$$

### 3 Solution method

The equations of motion are decoupled using both real and complex variables, and then rewritten in nondimensional form to facilitate the analysis of the effects of each governing parameter. Adopting a complex-variable approach, the general integral is sought by separation of time and space variables, yielding eigenfrequencies, closed-form expressions of the eigenfunctions, and critical speeds.

#### 3.1 Decoupling the equations of motion

Equations (13) can be rewritten as two coupled fourth-order (with respect to both  $x$  and  $t$ ) partial derivative equations with real coefficients and real variables  $v$  and  $w$ :

$$\langle \Phi_h | [\tilde{\mathcal{O}}] \Phi_k \rangle = \langle \Phi_k | [\mathcal{O}] \Phi_h \rangle \tag{18}$$

The two coupled fourth-order equations in the real variables  $\vartheta_y$  and  $\vartheta_z$  would be exactly the same as

Eq. (20), after substituting  $\vartheta_y$  with  $v$  and  $\vartheta_z$  with  $w$ . Equations (20) can be in turn decoupled into a single eighth-order (with respect to both  $x$  and  $t$ ) partial derivative equation in a real variable, as shown in “Appendix B”. They can also be decoupled into a single fourth-order (with respect to both  $x$  and  $t$ ) partial derivative equation with complex coefficients in a complex variable:

$$\begin{aligned} EJ \left( w^{IV} - \frac{\rho}{\kappa G} \dot{w}^{II} \right) - iT \left( w^{III} - \frac{\rho}{\kappa G} \dot{w}^I \right) - N\psi w^{II} \\ + \rho A \psi \ddot{w} - \rho J \left( \ddot{w}^{II} - \frac{\rho}{\kappa G} \ddot{w} \right) \\ + 2i\rho J \omega \left( \dot{w}^{II} - \frac{\rho}{\kappa G} \dot{w} \right) = 0 \end{aligned} \quad (21)$$

$$\begin{cases} \left( w^{IV} - \frac{\sigma}{\alpha^2} \ddot{w}^{II} \right) - i\hat{T} \left( w^{III} - \frac{\sigma}{\alpha^2} \dot{w}^I \right) - \hat{N} \alpha^2 \psi w^{II} + \psi \ddot{w} - \frac{1}{\alpha^2} \left( \ddot{w}^{II} - \frac{\sigma}{\alpha^2} \ddot{w} \right) + 2i \frac{\hat{\omega}}{\alpha^2} \left( \dot{w}^{II} - \frac{\sigma}{\alpha^2} \dot{w} \right) = 0 \\ \psi = 1 - \sigma \hat{N} \end{cases} \quad (24)$$

The decoupled fourth-order equation in the complex variable  $\theta$  would be exactly the same as Eq. (21), after substituting  $\theta$  with  $w$ . In Eq. (21) two complex coefficients identify the terms responsible of coupling the flexural behaviour in the  $x$ - $y$  and  $x$ - $z$  planes. These two coefficients would have opposite signs if adopting the complex variable  $w^* = v - iw$  instead of  $w$ , which would be the same as considering a counter-rotating shaft loaded by a clockwise twisting moment  $T$  (i.e. changing the sign to both  $\omega$  and  $T$ ). Notice that Eq. (21) would retain the same form also in the case of twisting moment  $T$  applied tangentially at the ends of the shaft (i.e. a follower torque). It generalizes the expressions given in [8] (effect of  $T$ ) and in [10] (effect of  $N$ ). The equation published in [12] is different, since the effects of  $N$  and  $T$  were introduced consistently with the Euler–Bernoulli beam model, rather than with the Timoshenko one.

### 3.2 Nondimensional form of the equations of motion

Considering a dimensionless spatial variable  $\xi$ , a dimensionless time  $\tau$  and a reference frequency parameter  $\Omega$  (which embodies the structural properties of the shaft):

$$\xi = \frac{x}{l}, \quad \tau = \Omega t, \quad \Omega = \frac{1}{l^2} \sqrt{\frac{EJ}{\rho A}} \quad (22)$$

and introducing the dimensionless parameters:

$$\begin{aligned} \alpha = \sqrt{\frac{Al^2}{J}} = \frac{2l}{r}, \quad \hat{\omega} = \frac{\omega}{\Omega}, \quad \sigma = \frac{E}{\kappa G}, \\ \hat{N} = \frac{N}{EA} \hat{T} = \frac{Tl}{EJ} \end{aligned} \quad (23)$$

where  $\alpha$  is the slenderness ratio, then any representation of the equations of motion of the rotating shaft can be rewritten in nondimensional form, as for instance Eq. (21):

In the case of a homogeneous shaft made of isotropic material with circular section, the shear elasticity modulus  $G$  and the shear factor  $\kappa$  can be expressed as functions of Young’s modulus and Poisson’s ratio [23]:

$$G = \frac{E}{2(1+\nu)}, \quad \kappa = \frac{6(1+\nu)}{7+6\nu} \Rightarrow \sigma = \frac{7+6\nu}{3} \quad (25)$$

hence the dimensionless parameter  $\sigma$  depends on Poisson’s ratio only, and within the limits of interest for the present study its variations are of minor importance. As a consequence, the equations of motion of the rotating shaft depend on just four parameters of major interest: slenderness ratio  $\alpha$ , dimensionless angular speed  $\hat{\omega}$ , dimensionless axial end thrust  $\hat{N}$  and dimensionless twisting moment  $\hat{T}$ .

### 3.3 Differential eigenproblem for complex displacements

The general integral is sought by modal analysis, solving a differential eigenproblem. In this respect, the most convenient form of the equations of motion to deal with is the complex-variable, decoupled fourth-



order Eq. (24). It is rewritten by separating the time and space variables and Laplace transforming with respect to time:

$$w(\xi, \tau) = \phi_w(\xi) \eta(\tau) \Rightarrow L(w) = \phi_w(\xi) \eta(s) \Rightarrow p_4 \phi_w^{IV} + p_3 \phi_w^{III} + p_2 \phi_w^{II} + p_1 \phi_w^I + p_0 \phi_w = 0 \tag{26}$$

where the five complex coefficients  $p$  read:

$$p_4 = 1, \quad p_3 = -i\hat{T},$$

$$p_2 = -\frac{1 + \sigma}{\alpha^2} s^2 + 2i \frac{\hat{\omega}}{\alpha^2} s - \psi \hat{N} \alpha^2, \tag{27}$$

$$p_1 = i\hat{T} \frac{\sigma}{\alpha^2} s^2, \quad p_0 = \frac{\sigma}{\alpha^4} s^4 - 2i \frac{\sigma \hat{\omega}}{\alpha^4} s^3 + \psi s^2$$

Notice that  $p_2, p_1$  and  $p_0$  depend on the eigenvalue  $s$ . The general integral of Eq. (24) can be expressed on the basis of the complex exponential function, yielding a characteristic polynomial equation with complex coefficients for the exponents  $a$ :

$$\phi_w(\xi) = B e^{a\xi}, \quad B, a \text{ complex}$$

$$\Rightarrow P(a) = \sum_{n=0}^4 p_n a^n = 0 \tag{28}$$

Closed-form expressions of the roots of the fourth-order polynomial equation  $P(a) = 0$  can be found by adopting either one of the classical solution methods or an advanced symbolic algebra software. The general integral is therefore expressed as a linear combination of four complex exponential functions:

$$\phi_w(\xi) = \sum_{n=1}^4 B_n e^{a_n \xi} \tag{29}$$

and the eigenvalues  $s$  can be computed after setting four boundary conditions. Assuming the same conditions at both ends of the shaft, the algebraic eigenproblem related to Eq. (29) takes the form:

$$\begin{bmatrix} b_1 & b_2 & b_3 & b_4 \\ c_1 & c_2 & c_3 & c_4 \\ b_1 e^{a_1} & b_2 e^{a_2} & b_3 e^{a_3} & b_4 e^{a_4} \\ c_1 e^{a_1} & c_2 e^{a_2} & c_3 e^{a_3} & c_4 e^{a_4} \end{bmatrix} \begin{bmatrix} B_1 \\ B_2 \\ B_3 \\ B_4 \end{bmatrix} = \mathbf{0} \tag{30}$$

where the first two equations represent the conditions in  $\xi = 0$ , and the following two the conditions in  $\xi = 1$ . The complex coefficients  $b$  and  $c$  depend on the

kind of boundary conditions and in the more general case they are explicit functions of both the exponents  $a$  and the eigenvalues  $s$ . Setting to zero the determinant of the coefficient matrix in Eq. (30) yields the characteristic equation for the eigenvalues  $s$ :

$$\Delta = D_{12} D_{34} [e^{a_1+a_2} + e^{a_3+a_4}] - D_{13} D_{24} [e^{a_1+a_3} + e^{a_2+a_4}] + D_{14} D_{23} [e^{a_1+a_4} + e^{a_2+a_3}] = 0, \tag{31}$$

$$D_{nm} = b_n c_m - b_m c_n$$

which is a complex function of the complex variable  $s$ . However, pure imaginary eigenvalues, i.e.  $s = i\lambda$ , can be numerically computed by using a zero-find routine of a real function  $f$  of the real variable  $\lambda$ :

$$f[\Delta(i\lambda)] = 0, \quad \lambda \in (-\infty, +\infty) \tag{32}$$

The critical speeds  $\hat{\omega}_C = \omega_C/\Omega$  can be found by following the same procedure, setting  $\lambda = \hat{\omega}$  in Eq. (32) and solving it with respect to  $\hat{\omega}$ , while the eigenfunctions for the complex angular displacement  $\theta$  can be expressed in the form:

$$\phi_\theta(\xi) = \frac{i}{l} \sum_{n=1}^4 B_n R_n(\lambda) e^{a_n \xi}, \tag{33}$$

$$R_n(\lambda) = \frac{1}{\psi a_n} \left( a_n^2 + \frac{\sigma \lambda^2}{\alpha^2} \right)$$

The solution of the adjoint problem can be immediately found by considering the adjoint operators in Eq. (19) and a characteristic polynomial  $\tilde{P}(a)$  defined by coefficients  $\tilde{p}$ , equal to those in Eq. (27), except for changing the sign to both  $\omega$  and  $T$ , or considering the complex variable  $w^* = v - iw$  instead of  $w$ , as noticed in Sect. 3.1. The eigenvalues are the same as those computed through Eq. (32), but with opposite signs ( $\tilde{\lambda} = -\lambda$ ), since the characteristic equation in this case would be  $f[\Delta(-i\tilde{\lambda})] = 0$ .

### 3.4 Boundary conditions for complex displacements

Isotropic supports are considered, hence the boundary conditions associated to Eq. (24) can be expressed as functions of the complex variable  $w$  alone, due to axial symmetry. In the simplest configurations they read:

*Clamped end*, case with null rotations and null shear deformations:

shear effect and twisting moment in the equations of motion.

$$\begin{cases} v = w = 0 \\ \vartheta_y + \gamma_y + \beta_y = 0, \quad \vartheta_z + \gamma_z + \beta_z = 0 \end{cases} \Rightarrow \begin{cases} w = 0 \\ w^I = 0 \end{cases} \quad (34)$$

*Clamped end*, case with null rotations only:

$$\begin{cases} v = w = 0 \\ \vartheta_y = \vartheta_z = 0 \end{cases} \Rightarrow w = 0, \quad w^I + \frac{\sigma}{\psi \alpha^2} \left[ \left( w^{III} - \frac{\sigma}{\alpha^2} \dot{w}^I \right) - i\hat{T} w^{II} - \psi \hat{N} \alpha^2 w^I \right] = 0 \quad (35)$$

*Simply supported end*, case with  $T = 0$  or case with tangential  $T$  (follower torque):

#### 4 Modal analysis

$$\begin{cases} v = w = 0 \\ M_y = M_z = 0 \end{cases} \Rightarrow \begin{cases} w = 0 \\ w^{II} = 0 \end{cases} \quad (36)$$

After clarifying the relation between eigensolutions obtained for complex and real displacement variables, modal analysis of the rotating shaft is then completed using real displacement variables in both the config-

*Simply supported end*, case with axial  $T$ :

$$w = 0, \quad w^{II} - i\hat{T} w^I - \frac{\sigma}{\psi \alpha^2} \left[ i\hat{T} \left( w^{III} - \frac{\sigma}{\alpha^2} \dot{w}^I - i\hat{T} w^{II} - \psi \hat{N} \alpha^2 w^I \right) - \frac{1}{\alpha^2} (\ddot{w}^{II} - 2i\hat{\omega} \dot{w}^{II}) \right] = 0 \quad (37)$$

*Free end*:

$$\begin{cases} M_y = M_z = 0 \\ F_y = F_z = 0 \end{cases} \Rightarrow \begin{cases} \left( w^{II} - \frac{\sigma}{\alpha^2} \ddot{w} \right) - i\hat{T} w^I - \psi \hat{N} \alpha^2 w = 0 \\ \left( w^{III} - \frac{\sigma}{\alpha^2} \dot{w}^I \right) - i\hat{T} \left( w^{II} - \frac{\sigma}{\alpha^2} \dot{w} \right) - \psi \hat{N} \alpha^2 w^I - \frac{1}{\alpha^2} (\ddot{w}^I - 2i\hat{\omega} \dot{w}^I) = 0 \end{cases} \quad (38)$$

Introducing Eq. (29) into the selected boundary equations gives the expressions of the coefficients  $b$  and  $c$  of the characteristic Eq. (31). Notice that the second of Eq. (37) generalizes the expression given in [8] (with opposite sign convention for  $T$ ), and that in [12] the terms in square brackets are omitted, as a consequence of disregarding the interaction between

uration space and in the state-space, including the derivation of critical loads due to combined effects of axial end thrust and twisting moment.

4.1 Differential eigenproblem for real displacements

Decoupling the four second-order equations of motion, Eq. (13), into a single eighth-order equation in a real variable, as shown in “Appendix B”, separating the time and space variables and then Laplace transforming with respect to time as done in Eq. (26) gives:

$$q_8\phi^{VIII} + q_7\phi^{VII} + q_6\phi^{VI} + q_5\phi^V + q_4\phi^{IV} + q_3\phi^{III} + q_2\phi^{II} + q_1\phi^I + q_0\phi = 0 \tag{39}$$

whose general integral can be represented on the basis of the complex exponential function, yielding a characteristic polynomial equation with complex coefficients for the exponents  $a$ :

$$\phi(\xi) = C e^{a\xi}, \quad C, a \text{ complex} \Rightarrow Q(a) = \sum_{n=0}^8 q_n a^n = 0 \tag{40}$$

The eighth-grade polynomial  $Q(a)$  factorizes into the two fourth-grade polynomials  $P(a)$  and  $\tilde{P}(a)$ , then the coefficients  $q$  (reported in “Appendix B”) can also be expressed as functions of the coefficients  $p$  and  $\tilde{p}$  in the form of a convolution sum:

$$Q(a) = P(a)\tilde{P}(a) \Rightarrow q_n = \sum_{m=0}^n p_m \tilde{p}_{n-m} \quad \text{with} \quad p_n = \tilde{p}_n = 0 \quad \text{for} \quad n > 4 \tag{41}$$

The same characteristic equation  $Q(a) = 0$  could be obtained directly from Eq. (13), assuming as a basis the complex exponential function in the following vector representation:

$$\phi(\xi) = \Phi_0 e^{a\xi}, \quad \Phi_0 = \{ C_v \quad C_w \quad C_{\vartheta_y} \quad C_{\vartheta_z} \}^T, \quad C, a \text{ complex} \tag{42}$$

which, introduced in the Laplace transformed operator form of the equations of motion, Eq. (14), gives:

$$s^2 \mathbf{M} \phi + s \mathbf{G} \phi + [\mathcal{K}] \phi = \mathbf{0} \Rightarrow \mathbf{D}(s, a) \phi_0 = \mathbf{0} \tag{43}$$

where:

$$\mathbf{D} = \begin{bmatrix} d_1 & 0 & 0 & -d_4 \\ 0 & d_1 & d_4 & 0 \\ 0 & -d_4 & d_3 & d_2 \\ d_4 & 0 & -d_2 & d_3 \end{bmatrix}, \tag{44}$$

$$d_1 = a^2 - \frac{\sigma s^2}{\alpha^2}, \quad d_2 = \frac{\sigma}{\alpha^2} \left( \hat{T} a - 2 \hat{\omega} \frac{s}{\alpha^2} \right),$$

$$d_3 = \frac{\sigma}{\alpha^2} \left( a^2 - \frac{s^2}{\alpha^2} \right) - \psi, \quad d_4 = \psi a$$

Notice that in matrix  $\mathbf{D}$ , coefficients  $d_4$  are responsible of coupling between displacements and rotations on the same plane, while coefficients  $d_2$  couple

displacements and rotations in orthogonal planes. The latter are decoupled only when both  $T = 0$  and  $\omega = 0$ .

The algebraic eigenproblem in Eq. (43) can be solved by setting to zero the determinant of  $\mathbf{D}$ :

$$\begin{aligned} \det \mathbf{D} &= (d_1 d_3 + d_4^2)^2 + (d_1 d_2)^2 \\ &= \underbrace{[(d_1 d_3 + d_4^2) + i (d_1 d_2)]}_{P(a)} \underbrace{[(d_1 d_3 + d_4^2) - i (d_1 d_2)]}_{\tilde{P}(a)} \\ &= P(a)\tilde{P}(a) = 0 \end{aligned} \tag{45}$$

which is the same characteristic equation for the eight exponents  $a$  given by Eq. (40). Therefore the eigenvalues  $s = \pm i\lambda$  associated to the eighth-order

problem are all those computed solving  $f[\Delta(i\lambda)] = 0$ , Eq. (32), plus those computed solving  $f[\Delta(-i\lambda)] = 0$ , i.e. the adjoint fourth-order problem as discussed in Sect. 3.3. If both  $T = 0$  and  $\omega = 0$  (i.e.  $d_2 = 0$ ), then Eq. (20) are decoupled, and the sets of eigenvalues associated to the two fourth-order problems are coincident, meaning that in this case each eigenvalue has multiplicity 2.

#### 4.2 Expression of the eigenfunctions for real displacements

According to the eigenproblem formulation in Sect. 4.1, the four scalar eigenfunctions for the real displacements  $v, w, \vartheta_y, \vartheta_z$  can be expressed as:

$$\begin{aligned} \phi_v(\xi) &= \sum_{n=1}^8 C_{nv} e^{a_n \xi}, & \phi_w(\xi) &= \sum_{n=1}^8 C_{nw} e^{a_n \xi}, \\ \phi_{\vartheta_y}(\xi) &= \sum_{n=1}^8 C_{n\vartheta_y} e^{a_n \xi}, & \phi_{\vartheta_z}(\xi) &= \sum_{n=1}^8 C_{n\vartheta_z} e^{a_n \xi} \end{aligned} \tag{46}$$

Relations among the four amplitude constants  $C_n$  as functions of one of them (say  $C_{nv}$ ) can be found recalling the algebraic eigenproblem in Eq. (43), along with the definitions in Eqs. (42) and (44). For any given eigenvalue  $s = i\lambda$  and for an exponent  $a_n(i\lambda)$ , two possible expressions for the eigenvector  $\phi_{0n}$  can be found:

$$\begin{aligned} \phi_{0n} &= C_{nv} \{ 1 \quad +i \quad -iR_n \quad R_n \}^T \quad \text{or} \\ \tilde{\phi}_{0n} &= C_{nv} \{ 1 \quad -i \quad +iR_n \quad R_n \}^T \end{aligned} \tag{47}$$

where  $R_n = d_1/d_4$  with  $s = i\lambda$ , according to the definition given in Eq. (33). The meaning of these two possible solutions is clarified after introducing one of them (say  $\phi_{0n}$ ) in the system Eq. (43), obtaining:

$$\begin{cases} d_1 - d_4 R_n = 0 \\ i(d_1 - d_4 R_n) = 0 \\ -i(d_4 + d_3 R_n + i d_2 R_n) = 0 \\ d_4 + d_3 R_n + i d_2 R_n = 0 \end{cases} \Leftrightarrow \underbrace{(d_1 d_3 + d_4^2) + i(d_1 d_2)}_{P(a)} = 0 \tag{48}$$

where the system is reduced to just two independent equations; introducing the first equation into the fourth one yields the characteristic equation in terms of  $P(a)$ . Clearly, the other eigenvector in Eq. (47) would lead

to the characteristic equation in terms of  $\tilde{P}(a)$ , associated to the adjoint problem. As a consequence, the eigenfunctions in Eq. (46) can be expressed in terms of two sets of amplitude constants, four of them given by  $\phi$  and the other four by its adjoint  $\tilde{\phi}$ . The relations between real displacement eigenfunctions and complex displacement eigenfunctions can then be found recalling the definitions in Eqs. (29), (46) and (47):

$$\begin{aligned} \phi_w &= \sum_{n=1}^4 B_n e^{a_n \xi} = \phi_v + i \phi_w \\ &= \sum_{n=1}^8 (C_{nv} + i C_{nw}) e^{a_n \xi} \\ &= \sum_{n=1}^8 [C_{nv} + i(\pm i C_{nv})] e^{a_n \xi} \\ &= 2 \sum_{n=1}^4 C_{nv} e^{a_n \xi} = 2\phi_v \end{aligned} \tag{49}$$

where four out of eight terms in the sum vanish due to opposite signs in  $\phi$  and  $\tilde{\phi}$ . This result was expected: being  $\phi_w$  a linear combination of four complex exponentials, also  $\phi_v$  should result as a linear combination of four complex exponentials. Following the same steps, starting from  $\phi_\theta$  for the angular displacement eigenfunctions, the four relations between real displacement eigenfunctions and complex displacement eigenfunctions can be given in the form:

$$\begin{aligned} \phi_v &= \frac{\phi_w}{2}, & \phi_w &= -i \frac{\phi_w}{2}, \\ \phi_{\vartheta_y} &= \frac{\phi_\theta}{2}, & \phi_{\vartheta_z} &= -i \frac{\phi_\theta}{2} \end{aligned} \tag{50}$$

Also this result was expected, due to symmetry: the only difference between for instance  $\phi_v$  and  $\phi_w$  is a phase-lag consisting in a  $\pi/2$  delay of  $\phi_w$  with respect

$$\lim_{\kappa \rightarrow \infty} R_n = a_n \Rightarrow \lim_{\kappa \rightarrow \infty} \phi_\theta = \frac{i}{l} \sum_{n=1}^4 a_n B_n e^{a_n \xi} \Rightarrow \lim_{\kappa \rightarrow \infty} \theta = \frac{i w^I}{l} \Rightarrow \lim_{\kappa \rightarrow \infty} \vartheta_y = -\frac{w^I}{l}, \quad \lim_{\kappa \rightarrow \infty} \vartheta_z = \frac{v^I}{l} \tag{51}$$

to  $\phi_v$ . Notice that for  $\kappa \rightarrow \infty$ , Eq. (50) together with Eq. (33) yield a result consistent with the Euler–Bernoulli and Rayleigh models, and with Eq. (2): where the dimensional factor at the denominator is related to differentiation with respect to the dimensionless spatial variable  $\xi$ .

### 4.3 Biorthogonality relations

The vectors of lagrangian coordinates in the configuration space  $\mathbf{q}$  and in the state-space  $\mathbf{q}_s$ , can be expressed as linear combinations of eigenfunctions  $\phi$  and state-space eigenfunctions  $\Phi$  respectively, according to:

$$\mathbf{q} = \sum_{h=1}^{\infty} \phi_h \eta_h, \quad \mathbf{q}_s = \sum_{h=1}^{\infty} \Phi_h \eta_h, \quad \Phi_h = \begin{Bmatrix} \phi_h \\ s_h \phi_h \end{Bmatrix} \tag{52}$$

Considering nondimensional operators, the non-homogeneous state-space representation in the Laplace domain of the second-order differential equations of motion, Eq. (13), reads:

$$s \hat{\mathbf{A}} \mathbf{q}_s + [\hat{\mathcal{B}}] \mathbf{q}_s = \hat{\mathbf{f}}_s \tag{53}$$

Since the eigenfunctions and the adjoint eigenfunctions are bi-orthogonal, and they can be normalized as:

$$\begin{cases} \langle \tilde{\Phi}_h | \hat{\mathbf{A}} \Phi_k \rangle = \delta_{hk} \\ \langle \tilde{\Phi}_h | [\hat{\mathcal{B}}] \Phi_k \rangle = -s_h \delta_{hk} \end{cases}, \quad \delta_{hk} = \begin{cases} 1 & \text{if } h = k \\ 0 & \text{if } h \neq k \end{cases} \tag{54}$$

then multiplying Eq. (53) by the  $h$ th adjoint eigenfunction  $\tilde{\Phi}_h$  and integrating over the spatial domain gives:

$$s \langle \tilde{\Phi}_h | \hat{\mathbf{A}} \mathbf{q}_s \rangle + \langle \tilde{\Phi}_h | [\hat{\mathcal{B}}] \mathbf{q}_s \rangle = \langle \tilde{\Phi}_h | \hat{\mathbf{f}}_s \rangle \Leftrightarrow (s - s_h) \eta_h = f_h, \quad s_h = i \lambda_h \Leftrightarrow \eta_h = \frac{f_h}{s - i \lambda_h} \tag{55}$$

where  $f_h(s)$  is the  $h$ th resulting nondimensional modal force. Transforming Eq. (55) back to time domain gives the expression of the modal coordinate  $\eta_h(\tau)$  as a convolution integral. If  $f_h(s) = 1$ , then:

$$\eta_h(\tau) = e^{i \lambda_h \tau} \tag{56}$$

Considering now the real displacements related to a single vibration mode of the shaft, they can be expressed as:

$$v_h(\xi, \tau) = \phi_{vh} e^{i \lambda_h \tau} + \phi_{vh}^* e^{-i \lambda_h \tau} \tag{57}$$

therefore (dropping the subscript  $h$ ):

$$\begin{cases} v(\xi, \tau) = 2[\Re(\phi_v) \cos(\lambda \tau) - \Im(\phi_v) \sin(\lambda \tau)] \\ w(\xi, \tau) = 2[\Im(\phi_v) \cos(\lambda \tau) + \Re(\phi_v) \sin(\lambda \tau)] \\ \vartheta_y(\xi, \tau) = -2[\Im(\phi_{\vartheta_z}) \cos(\lambda \tau) - \Re(\phi_{\vartheta_z}) \sin(\lambda \tau)] \\ \vartheta_z(\xi, \tau) = +2[\Re(\phi_{\vartheta_z}) \cos(\lambda \tau) - \Im(\phi_{\vartheta_z}) \sin(\lambda \tau)] \end{cases} \tag{58}$$

The modal trajectory of each point of the elastic line of the shaft is always described by a circle of radius  $r_{el}(\xi)$ :

$$v^2(\xi, \tau) + w^2(\xi, \tau) = 4[\Re^2(\phi_v) + \Im^2(\phi_v)] = r_{el}^2(\xi) \tag{59}$$

since the phase-lag between its two components is always  $\pm \pi/2$ . If  $\lambda > 0$  (and  $\omega > 0$ ), then the modal elastic line rotates counter-clockwise about the  $x$  axis, therefore the  $\lambda > 0$  frequency values are usually referred to as forward natural frequencies; if  $\lambda < 0$  (and  $\omega > 0$ ), then the modal elastic line rotates

clockwise, and the  $\lambda < 0$  frequency values are usually referred to as backward natural frequencies. In the case  $|\hat{\omega}| = |\lambda|$ , a critical speed occurs only if  $\hat{\omega}\lambda > 0$ .

#### 4.4 Critical loads

In static conditions the characteristic equation for the exponents  $a$ , Eq. (28) with  $\lambda = 0$ , gives:

$$a_{1,2} = 0, \quad a_{3,4} = i \frac{\hat{T}}{2} \pm \begin{cases} \sqrt{-\Gamma} & \text{if } \Gamma < 0 \\ i\sqrt{\Gamma} & \text{if } \Gamma > 0 \end{cases}$$

with  $\Gamma = \frac{\hat{T}^2}{4} - \alpha^2 \psi \hat{N}$

(60)

For  $\hat{N} \neq 0$ , the  $w$  equilibrium equation, and its solution in terms of  $\phi_w$ , take the form:

$$EJw^{IV} - iTw^{III} - N\psi w^{II} = 0 \Rightarrow \phi_w(\xi) = B_1 e^{\alpha_1 \xi} + B_2 e^{\alpha_2 \xi} + B_3 \xi + B_4 = 0 \tag{61}$$

Applying the boundary conditions, considering for instance simply supported ends as in Eq. (36), yields the following results:

$$\begin{aligned} \Gamma \leq 0 &\Rightarrow B \sinh \sqrt{-\Gamma} = 0 \Rightarrow B = 0 \\ \Gamma > 0 &\Rightarrow B \sin \sqrt{\Gamma} = 0 \Rightarrow B = 0 \text{ or } \sqrt{\Gamma} = n\pi \end{aligned} \tag{62}$$

As a consequence, if  $\Gamma \leq 0$  the shaft does not bend; if  $\Gamma > 0$  the shaft bends at the critical equivalent loads:

$$\Gamma = n^2 \pi^2 \tag{63}$$

which, for  $\hat{T} = 0$  and  $\kappa \rightarrow \infty$  (i.e.  $\sigma = 0$ ,  $\psi = 1$ ), coincides with the well known expression of the critical buckling loads of the simply supported Euler–Bernoulli and Rayleigh beam models.

### 5 Discussion of the results

The effects of slenderness ratio  $\alpha$ , angular speed  $\hat{\omega}$ , axial end thrust  $\hat{N}$  and twisting moment  $\hat{T}$  are studied on natural frequencies, modal shapes and critical

speeds of the rotating shaft. Admissible ranges of variation for both  $\hat{N}$  and  $\hat{T}$  can be set recalling the definition of yield strength  $\sigma_{ys}$  of the homogeneous shaft material, and its link with the maximum value of  $\hat{N}$  (i.e.  $|\hat{N}_{max}| = \sigma_{ys}/E$ ). Hence a reasonable assumption can be  $|\hat{N}_{max}| < 0.01$ . Regarding  $|\hat{T}_{max}|$ , the Tresca criterion yields  $|\hat{T}_{max}| = \alpha |\hat{N}_{max}|/2$ . In some figures, however,  $\hat{T}$  has been increased up to exceedingly high values, to emphasize its effects and making more readable the plots.

#### 5.1 Natural frequencies

Natural frequencies are computed according to the procedure described in Sect. 3.3, through Eqs. (31) and (32). In the case  $\omega = 0$ , the absolute value of  $\Delta(i\lambda)$

is a symmetric function of the dimensionless parameter  $\lambda$ . Increasing the modulus of  $\hat{T}$  (positive or negative) reduces the modulus of natural frequencies  $\lambda$ , as shown in Fig. 3 (left). The same qualitative effect can be observed by increasing the modulus of a negative  $\hat{N}$  (compression), and the opposite by raising a positive  $\hat{N}$  (traction). In the case  $\omega \neq 0$ , the former symmetry is lost, and two spectra of natural frequencies are generated by considering  $\pm i\lambda$ . Increasing  $\hat{\omega}$  with  $\omega > 0$ , raises the natural frequencies  $\lambda$  as displayed in Fig. 3 (right, with  $\hat{N} = 0$  and  $\hat{T} = 0$ ). Increasing the modulus of  $\hat{\omega}$  with  $\omega < 0$ , in the case  $\hat{T} = 0$  causes the opposite (symmetric) effect, as explained at the end of Sect. 3.3 (the eigenvalues are the same as those computed through Eq. (32) with  $\omega > 0$ , but with opposite signs).

Considering now a simply supported rotating shaft with the following parameters:

$$\begin{aligned} \rho &= 7700 \text{ [Kg/m}^3\text{]}, \quad E = 210 \times 10^9 \text{ [Pa]}, \\ \nu &= 0.3, \quad r = 10 \text{ [mm]}, \\ l &= 250 \text{ [mm]}, \quad \omega = 1000 \text{ [rad/s]}, \\ \kappa &= 0.8864, \quad N = 0, \quad T = 0 \end{aligned}$$

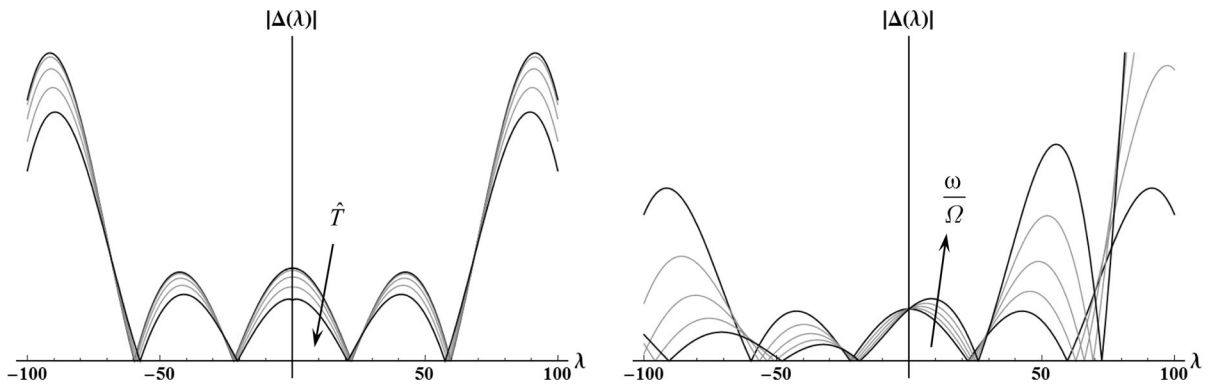


**Fig. 3** Absolute values  $|\Delta(\lambda)|$  of the characteristic function ( $\alpha = 50, \nu = 0.3$ , clamped ends with null rotations and shear deformations); left:  $\hat{T} > 0, \hat{\omega} = 0, \hat{N} = 0$ ; right:  $\hat{\omega} > 0, \hat{N} = 0, \hat{T} = 0$

**Table 1** First 4 natural frequencies  $\lambda\Omega$  [Hz] for a rotating unloaded simply supported shaft

	$\hat{\omega} > 0$				$\hat{\omega} < 0$			
	FEA—number of elements			DPM	FEA—number of elements			DPM
	1	5	10		1	5	10	
1	736.030	652.037	651.882	651.847	726.306	650.833	650.658	650.624
2	3351.66	2561.21	2552.27	2550.21	3330.78	2556.56	2547.73	2545.68
3	–	5652.63	5565.59	5544.83	–	5611.01	5556.45	5535.76
4	–	9931.85	9540.54	9440.12	–	9737.23	9526.28	9426.22

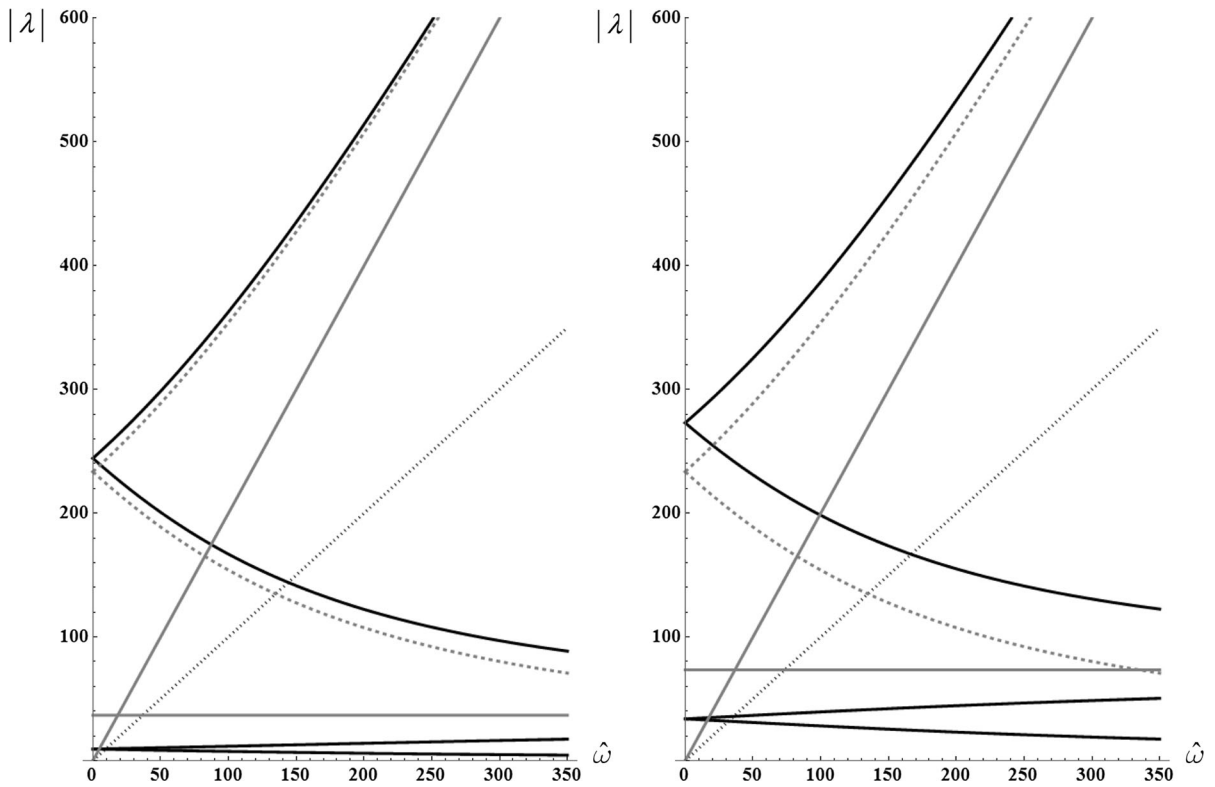
the first 4 positive natural frequencies  $\lambda\Omega$  of the two spectra, computed for the distributed parameter model (DPM) according to the method presented in Sect. 3.3, are reported in Tab. 1 ( $\alpha = 50$ , simply supported shaft) where they are compared with the results of a finite element analysis (FEA) using different numbers of Timoshenko rotating beam elements [20].

Figure 4 shows the absolute values  $|\lambda|$  (black continuous lines) of the two couples of eigenvalues related to  $n = 1$  (left) and  $n = 2$  (right) as functions of  $\hat{\omega}$ , with  $\alpha = 20, \nu = 0.3, \hat{N} = 0, \hat{T} = 0$  and simply supported ends. The asymptotic behaviour of the eigenvalues with respect to angular speed will be discussed in Sect. 5.3. The effects of external loads  $\hat{N}$  and  $\hat{T}$  on the lower natural frequencies are highlighted in Fig. 5, displaying differences [%] on the first (continuous lines) and second (dotted lines) positive natural frequencies  $\lambda$  of the forward spectrum, as functions of  $\hat{\omega}$ . These differences reduce progressively for increasing natural frequencies, and those due to  $\hat{T}$  are so small to be regarded as negligible.

### 5.2 Characteristic exponents

A qualitative analysis of the four exponents  $a$  in Eq. (29) highlights some important general aspects of modal shapes, independently from boundary conditions. The real and imaginary parts of the four roots of  $P(a)$ , Eq. (28), are displayed in 3D plots as functions of a continuous variable  $\lambda$ , representing all possible natural frequencies, as for instance reported in Figs. 6 and 7 for a rotating shaft with  $\alpha = 10, \hat{\omega} = 50, \hat{N} = \pm 0.005, \hat{T} = 0$  and  $\nu = 0.3$ .

If  $\hat{T} = 0$ , Eq. (28) is a biquadratic equation, with either two real opposite and two imaginary conjugate roots, or two pairs of imaginary conjugate roots. The diagrams, as in Figs. 6 and 7, are symmetric with respect to both the  $\lambda-\text{Re}(a)$  and  $\lambda-\text{Im}(a)$  planes. In the case of non-rotating shaft ( $\hat{\omega} = 0$ ) they would be symmetric also with respect to the  $\text{Re}(a)-\text{Im}(a)$  plane. Therefore the effect of angular speed is that of producing different values of  $a$  (and therefore of modal shapes) for forward and backward eigenfrequencies. Notice that the asymmetry between forward and backward modal shapes grows with increasing



**Fig. 4** Absolute values  $|\lambda|$  (black continuous lines) of the two couples of natural frequencies related to  $n = 1$  (left) and  $n = 2$  (right) as functions of  $\hat{\omega}$  ( $\alpha = 20, \nu = 0.3, \hat{N} = 0, \hat{T} = 0$ , simply

supported ends); grey continuous lines identify asymptotes, grey dotted curves identify switch frequencies

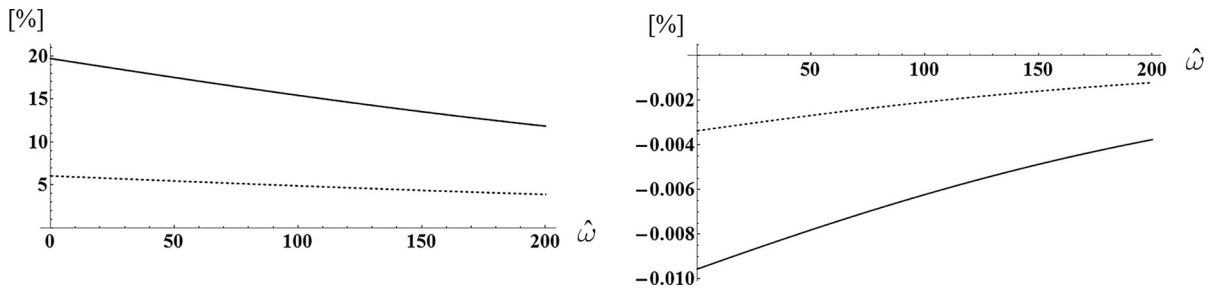


**Fig. 5** Differences due to external loads  $\hat{N}$  and  $\hat{T}$  on the first (continuous lines) and second (dotted lines) positive natural frequencies  $\lambda$  of the forward spectrum, as functions of  $\hat{\omega}$  ( $\alpha = 20, \nu = 0.3$ , simply supported ends); left: effect of the

maximum value of  $\hat{N} > 0$ , differences [%] with respect to the case  $\hat{N} = 0$ ; right: effect of the maximum value of  $\hat{T}$ , differences [%] with respect to the case  $\hat{T} = 0$

angular speed. The two non-zero frequency values for which two pairs of real roots  $a$  become null (and then switch to imaginary conjugate, in the following

referred to as switch frequencies) can be found by setting  $p_0 = 0$  in Eq. (27), yielding:

$$p(\lambda) = \frac{\sigma}{\alpha^4} \lambda^2 - 2 \frac{\sigma \hat{\omega}}{\alpha^4} \lambda - \psi = 0 \quad \Rightarrow \quad \begin{cases} \lambda_f = \hat{\omega} + \sqrt{\hat{\omega}^2 + \psi \alpha^4 \sigma^{-1}} \\ \lambda_b = \hat{\omega} - \sqrt{\hat{\omega}^2 + \psi \alpha^4 \sigma^{-1}} \end{cases} \quad (64)$$



**Fig. 6** The four roots of Eq. (32), exponents of the modal shapes, as functions of the natural frequencies  $\lambda$ , case with  $\hat{N} > 0$  ( $\hat{\omega} > 0$ ,  $\hat{T} = 0$ )

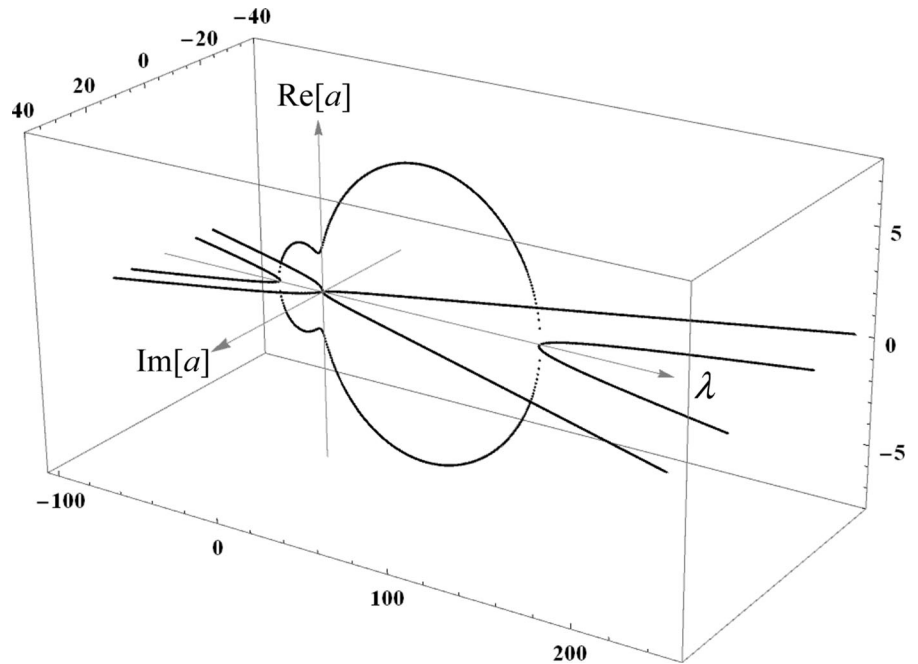
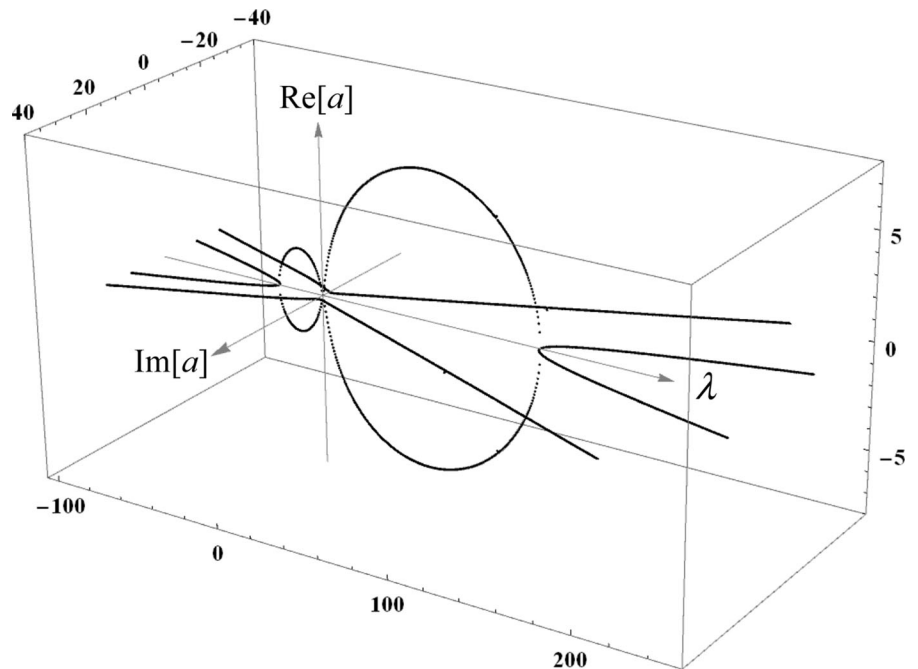


**Fig. 7** The four roots of Eq. (32), exponents of the modal shapes, as functions of the natural frequencies  $\lambda$ , case with  $\hat{N} < 0$  ( $\hat{\omega} > 0$ ,  $\hat{T} = 0$ )



Inside the interval defined by the two switch frequencies ( $\lambda_b, \lambda_p$ ), the modal shapes can be defined by combinations of hyperbolic and trigonometric functions; outside this range, the modal shapes are represented by trigonometric functions only. At the switch frequencies defined by Eq. (64) the

eigenfunctions take a peculiar form:  $\phi_w = 0$  (the elastic line does not bend) and  $\phi_\theta = \text{constant}$  (constant angular displacements along the spatial coordinate  $\xi$ ).

At zero natural frequency ( $\lambda = 0$ ), i.e. in static conditions, a traction axial thrust ( $\hat{N} > 0$ ) gives two non-zero opposite real values for  $a$  (Fig. 6), while a

compression axial thrust ( $\hat{N} < 0$ ) gives two non-zero pure imaginary conjugate values (Fig. 7); in the former case the shaft does not bend, in the latter case the shaft bends at critical loads, as discussed in Sect. 4.4.

If a twisting moment acting on the shaft is considered ( $\hat{T} \neq 0$ ), then the only preserved plane of symmetry is the  $\lambda$ -Im( $a$ ) plane. Symmetry with respect to the  $\lambda$ -Re( $a$ ) plane is lost, as shown in Fig. 8 for a rotating shaft with  $\alpha = 10$ ,  $\hat{\omega} = 50$ ,  $\hat{N} = 0$ ,  $\nu = 0.3$  and several increasing values of  $\hat{T} > 0$ . In Fig. 8 (left), to emphasize the effects of  $\hat{T}$  on the overall behaviour of the roots  $a$  in the  $\lambda$ -Im( $a$ ) plane, the twisting moment is increased up to exceedingly high values, the represented map retaining mathematical meaning only. In static conditions ( $\lambda = 0$ ), for  $\hat{N} = 0$   $P(a)$  yield a single non-zero imaginary root ( $a = i\hat{T}$ ). In Fig. 8 (right), a small portion of the same

plot is displayed, around the forward switch frequency values, varying  $\hat{T}$  in a realistic range until  $|\hat{N}_{\max}| = 0.01$ . It can be observed that absolute values of switch frequencies are reduced with increasing  $|\hat{T}|$ , and that inside the whole interval defined by a forward and a backward switch frequency, a pair of exponents  $a$  become complex-valued (for realistic values of  $\hat{T}$ , however, such reduction of switch frequencies, as well as the imaginary parts of complex  $a$ , are very slight). The points in which the curves cross the  $\lambda$ -axis are independent from  $\hat{T}$ , and it can be demonstrated that their frequency values are still given by Eq. (64). In these points (and not at the actual switch frequencies for  $\hat{T} \neq 0$ ), the modal shapes retain the already described peculiar features ( $\phi_w = 0$  and  $\phi_\theta = \text{constant}$ ).

Regarding the behaviour at high frequency, it turns out that in the most general case ( $\hat{\omega} \neq 0, \hat{N} \neq 0, \hat{T} \neq 0$ )

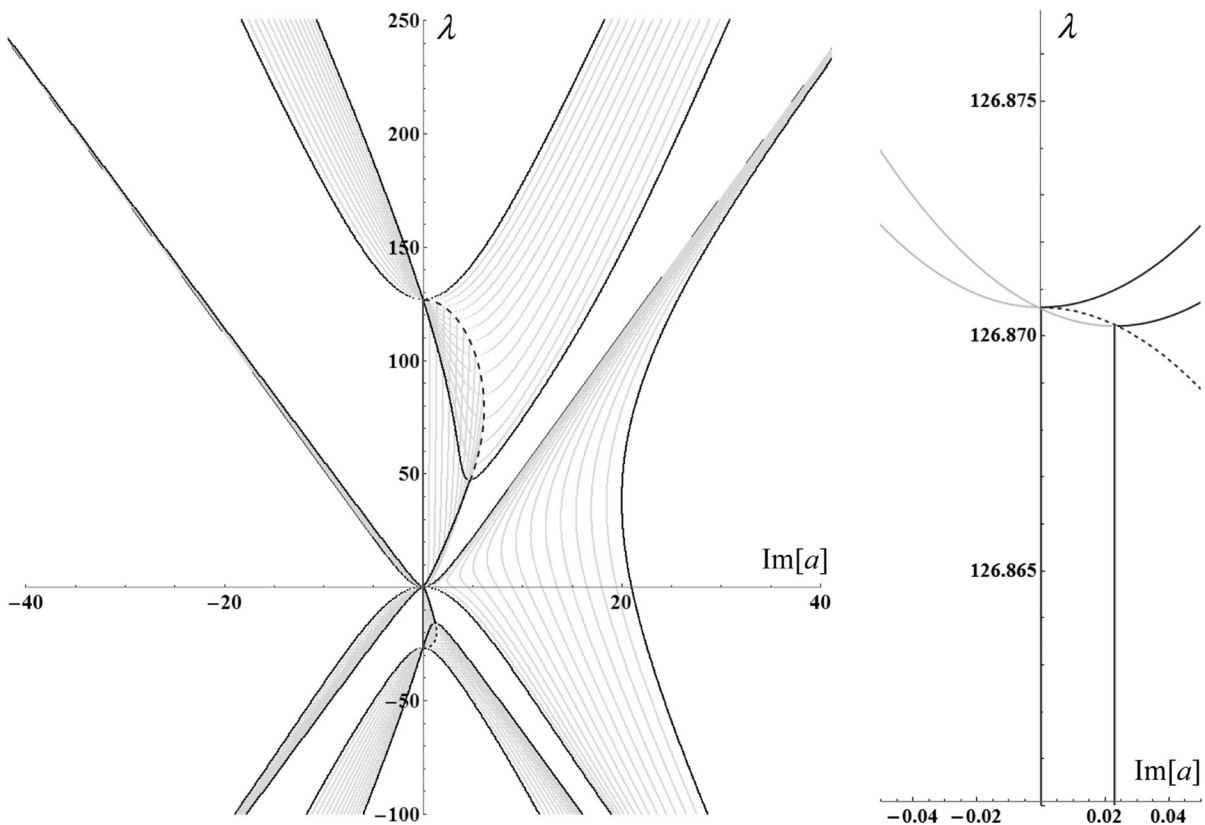


**Fig. 8** The imaginary parts of the four roots of Eq. (27), exponents of the modal shapes, as functions of the natural frequencies  $\lambda$ ; left: overall diagram with several increasing

values of  $\hat{T} > 0$  ( $\hat{\omega} > 0, \hat{N} = 0$ ); right: detail of the position of switch points for realistic values of  $\hat{T} > 0$

the pairs of conjugate imaginary roots  $a$  are asymptotic to straight lines, given by:

$$\begin{aligned}
 a &= \pm i \frac{\sqrt{\sigma}}{\alpha} \lambda \quad \text{always pure imaginary roots} \\
 a &= \pm \frac{i}{\alpha} \lambda \quad \text{pure imaginary roots beyond the switch frequencies}
 \end{aligned}
 \tag{65}$$

which depend strongly on slenderness ratio  $\alpha$  and on a lesser extent on Poisson’s ratio  $\nu$  ( $\sigma$ ), but they are totally independent from  $\hat{\omega}$ ,  $\hat{N}$  and  $\hat{T}$ . Therefore the effects of rotating speed and external loads are the largest on lower modes, while progressively fading away at increasing frequencies.

or  $\lambda \rightarrow 0$ , in which case Eq. (13) reduce to Eq. (3) (null acceleration) and its homologous for  $w$ :

$$\begin{aligned}
 \omega \rightarrow \infty \\
 \lambda \rightarrow 0 \quad \Rightarrow \quad \begin{cases} v^{\text{II}} - \psi v_z^{\text{I}} = 0 \\ w^{\text{II}} + \psi v_y^{\text{I}} = 0 \end{cases}
 \end{aligned}
 \tag{67}$$

If, on the other hand, eigenvalues tend to infinity with angular speed, dividing the third and fourth of Eq. (15) by  $\omega^2$  and letting both  $\omega \rightarrow \infty$  and  $\lambda \rightarrow \infty$  gives:

$$\begin{aligned}
 \omega \rightarrow \infty \\
 \lambda \rightarrow \infty \quad \Rightarrow \quad \lambda = k_{\infty} \omega \quad \text{with} \quad \begin{cases} k_{\infty} = 2 & \text{if } I_x = 2J, \quad I_y = I_z = J \\ k_{\infty} = I_x/J & \text{if } I_y = I_z = J \end{cases}
 \end{aligned}
 \tag{68}$$

### 5.3 Second spectrum and switch frequencies

The asymptotic behaviour of the eigenvalues with respect to angular speed of the rotating shaft ( $\omega \rightarrow \infty$ , as shown in Fig. 4, grey continuous lines), can be studied in a general case.

Considering the equations of motion Eq. (13), dividing the third and fourth equations by  $\omega$  and letting  $\omega \rightarrow \infty$ , then all terms on the third and fourth rows of operators  $\mathbf{M}$  and  $[\mathcal{K}(\cdot)]$ , Eqs. (15–16), tend to 0. Consequently, if eigenvalues tend to finite values, there are two possible cases: either  $\lambda \rightarrow \lambda_{\infty}$ ,  $\lambda_{\infty} \neq 0$ , in which limit case Eq. (13) yield:

which could be obtained directly referring to the equilibrium represented in Fig. 2B. Therefore the asymptotic behaviour of the forward and backward natural frequencies of the rotating shaft can be summarized as:

$$\omega \rightarrow \infty \quad \Rightarrow \quad \begin{cases} \lambda = 0, & \text{horizontal asymptote} \\ |\lambda| = \frac{\alpha}{\sqrt{\sigma}} a_{\infty n}, & \text{horizontal asymptote} \\ \lambda \rightarrow \infty, & \text{asymptotic to } \lambda = k_{\infty} \omega \end{cases}
 \tag{69}$$

$$\omega \rightarrow \infty \quad \Rightarrow \quad \begin{cases} \vartheta_y = 0 \\ \vartheta_z = 0 \end{cases} \quad \Rightarrow \quad \begin{cases} \rho A \ddot{v} - \kappa G A v^{\text{II}} = 0 \\ \rho A \ddot{w} - \kappa G A w^{\text{II}} = 0 \end{cases} \quad \Rightarrow \quad |\lambda_{\infty}| = \frac{\alpha}{\sqrt{\sigma}} a_{\infty n}, \quad a_{\infty n} = \sqrt{-I^2 \frac{\langle \phi_{v,n}, v^{\text{II}} \rangle}{\langle \phi_{v,n}, v \rangle}}
 \tag{66}$$

where  $n$  identifies the mode order. Notice that the horizontal asymptotes in Eq. (69) correspond to the straight asymptotic lines defined in the first of Eq. (65), which in the case of finite eigenvalues are reached as  $\omega \rightarrow \infty$ . Notice also that the asymptotic behaviour does not depend on the external loads  $N$  and  $T$ , and that for a shaft with same boundary conditions at both ends, from Eq. (66) it results simply  $a_{\infty n} = n\pi$  as in the case of Fig. 4. Each non-zero horizontal asymptote represents a link between two pairs of eigenvalues, one pair at lower frequencies, one pair at higher frequencies. The latter, when  $\omega = 0$  and in particular cases of boundary conditions in which the characteristic equation factorizes (as in the case of simply supported ends), can be identified with what is referred to as Timoshenko (beam theory) second spectrum [14]. The existence of such second spectrum in the case of general boundary conditions has been debated in the literature [15, 16], since when  $\omega = 0$  it is possible to easily identify the companion natural frequencies constituting the second spectrum only in particular cases, while finite element simulations produced conflicting conclusions [17]. More recently, the existence of a second spectrum in a non-rotating finite-length beam has been demonstrated on the basis of accurate experimental results, at least for free–free boundary conditions [18], and also by considering free waves in beams of infinite length, modelled according to the Timoshenko theory, showing the existence of two distinct frequency branches for any wavenumber [19].

However, when considering a rotating shaft, as  $\omega \rightarrow \infty$  the existence of non-zero horizontal asymptotes for any boundary conditions suggests a new way for defining and identifying the natural frequencies of the Timoshenko first and second spectra. All first spectrum backward eigenfrequencies tend to 0; all second spectrum forward eigenfrequencies tend to infinity, asymptotic to  $\lambda = k_{\infty}\omega$ , while the absolute value of each first spectrum forward eigenfrequency converges to the backward companion one belonging to the second spectrum. Therefore, the first spectrum can be identified by setting  $\lambda = k\hat{\omega}$ ,  $0 < k \leq k_{\infty}$  in Eq. (32) and solving it with respect to  $\hat{\omega}$ . The solutions identify the curves (or branches) of the first spectrum forward eigenvalues, since those of the second spectrum do not intersect any of the lines  $\lambda = k\hat{\omega}$ ,  $0 < k \leq k_{\infty}$ , as for example shown in

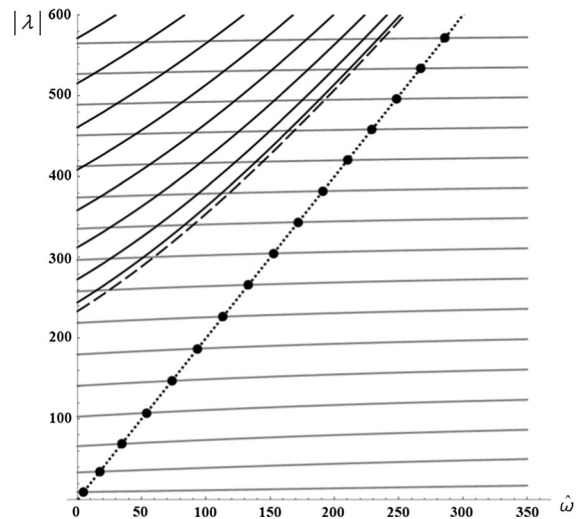


**Fig. 9** Absolute values  $|\lambda|$  of forward natural frequencies as functions of  $\hat{\omega}$  ( $\alpha = 10$ ,  $\sigma = 2.933$ ,  $\hat{N} = \hat{T} = 0$ ); the dotted line identifies the asymptote  $\lambda = 2\omega$ , the dashed curve identify the forward switch frequencies

Fig. 9. As a consequence, notice also that the whole second spectrum gives no contribution to the forward critical speeds. The problem of identifying the first spectrum frequencies at a given angular speed (eventually at  $\omega = 0$ ) can then be solved by using an iterative procedure (Rayleigh quotient) able to follow each identified branch to the desired value of angular speed.

Recalling now the switch frequencies defined in Eq. (64), in the case of non-rotating unloaded Timoshenko beams they reduce to a unique value  $\lambda = \alpha^2/\sqrt{\sigma}$ . This critical value is sometimes referred to as cut-off frequency [16, 17], while Eq. (64) generalizes its definition to the rotating and axially loaded case; if considering also a twisting moment, for realistic values of  $\hat{T}$  Eq. (64) can be considered a good approximation of the switch frequencies, as shown in Sect. 5.2, and it still gives the exact frequency values in which no-total-deflection modal shapes occur ( $\phi_w = 0$  and  $\phi_\theta = \text{constant}$ ). Clearly, the most influential parameter on the switch frequencies is the slenderness ratio  $\alpha$ ; however  $\hat{\omega}$  can influence significantly  $\lambda_f$  and  $\lambda_b$  at high speed, while the effect of external loads in this case is of minor importance.

Figure 4 shows the two switch frequencies ( $\lambda_b$ ,  $\lambda_f$ ) as functions of  $\hat{\omega}$  (grey dotted curves, case with  $\alpha = 20$ ,  $\nu = 0.3$ ,  $\hat{N} = 0$ ,  $\hat{T} = 0$  and simply supported ends). From Eq. (64) it can be found that as  $\omega \rightarrow \infty$

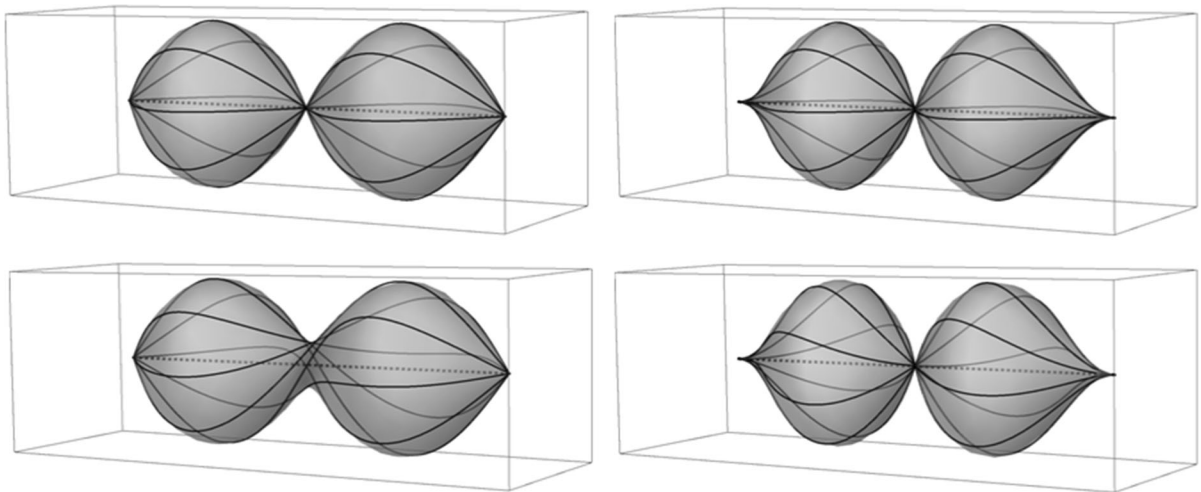


**Fig. 10** Second forward modal shape for the elastic line, with  $\alpha = 50$ ,  $\hat{\omega} = 10$ ,  $\hat{N} = 0$  and  $\nu = 0.3$ ; left column: simply supported ends, Eq. (36); right column: clamped ends, Eq. (34); upper row,  $\hat{T} = 0$ ; lower row,  $\hat{T} = 5$

then  $\lambda_b \rightarrow 0$  and  $\lambda_f \rightarrow +\infty$ . It can also be observed that the switch frequency curve is asymptotic to  $\lambda = k_\infty \hat{\omega}$  (as shown in Figs. 4 and 9) and that all the branches of the first spectrum natural frequencies cross the switch frequency curve twice (forward and backward), while those of the second spectrum always lay above it (the switch frequency curve is not a boundary between the two frequency spectra, it is a lower bound for the second frequency spectrum). Therefore, at any given angular speed, all the forward eigenvalues smaller than the switch value (at that angular speed) belong to the first frequency spectrum. Above the switch value the frequencies of the two spectra overlap in some complicated fashion, however they can be identified in general by following the criterion given above.

As already noticed in Sect. 5.2, at the switch frequencies the total deflection angles are zero, consequently the shear angles and the cross-section rotation angles are in counter-phase (equal and opposite if  $\psi = 1$ ), as it can be understood from the expression of the shear angle eigenfunctions  $\phi_{\gamma_z}$ :

$$\phi_{\gamma_z} = \phi_v^I - \psi \phi_{\vartheta_z} = -\frac{\sigma \lambda^2}{2l\alpha^2} \sum_{n=1}^4 \frac{B_n}{a_n} e^{a_n \zeta} \tag{70}$$

obtained from Eqs. (2), (29), (33) and (50). On the other hand, as  $\omega \rightarrow \infty$  at the horizontal asymptotes the cross-section rotation angles become zero, consequently the shear angles and the total deflection angles are in-phase (actually they coincide). Therefore,

increasing the angular speed and following a first spectrum forward branch which intersect the switch frequencies curve, changes are observed in phase relations among cross-section rotation, shear angle and total slope.

As discussed in the literature, above the cut-off frequencies the results given by the Timoshenko beam theory become progressively less accurate. According to some authors, the whole second spectrum should be disregarded, and considered un-physical [16, 17], in contrast with the results presented in [18, 19]. In any case, it should be noticed that the frequency range of validity of the model under analysis is reduced if considering small values of slenderness ratio  $\alpha$ , and this is related to the fact that, beyond certain frequency limits, the assumption of planarity of cross-sections during deformation clearly becomes unrealistic.

### 5.4 Modal shapes

Modal shapes for the variables in the configuration space are determined through Eqs. (29), (33), (50) and (58), taking into account some additional remarks about representation of angular displacements, as reported in “Appendix C”. As an example, in Fig. 10 the second forward modal shapes for the elastic line are displayed, for both simply supported and clamped ends, highlighting the twisting effects of  $\hat{T}$  (emphasized by increasing its value up to exceedingly high values, for the sake of readability). While in Fig. 11

the whole second modal shape is represented, for the simply supported unloaded rotating shaft.

Notice that forward and backward modal shapes are different, as for instance results from Figs. 6, 7 and 8, due to a lack of symmetry with respect to the  $\text{Re}(a)$ – $\text{Im}(a)$  plane.

### 5.5 Critical speeds

Critical speeds are computed according to the procedure described in Sect. 3.3, through Eqs. (31) and (32). Campbell 2D diagrams are shown in Fig. 4,

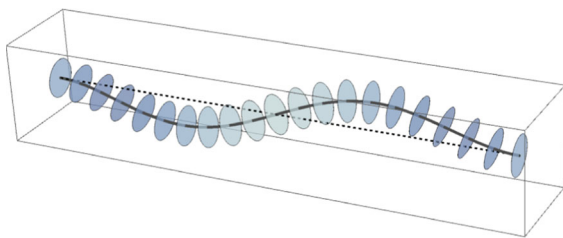


**Fig. 11** Second forward modal shape, with  $\alpha = 50$ ,  $\hat{\omega} = 10$ ,  $\hat{N} = 0$ ,  $\hat{T} = 0$  and  $\nu = 0.3$

where straight dotted lines represent the condition  $\lambda = \hat{\omega}$ . However, the effects of the main governing parameters on critical speeds are better highlighted by the diagrams displayed in Fig. 12. There the square root of the first nondimensional forward critical speed  $\sqrt{\hat{\omega}_{C1}}$  of a rotating shaft with  $\nu = 0.3$  and clamped ends (null rotations and shear deformations) is represented as a function of the slenderness ratio  $\alpha$ , for different values of  $\hat{T}$  in combination with  $\hat{N} = 0$  (left),  $\hat{N} > 0$  (center) and  $\hat{N} < 0$  (right).

Increasing the modulus of  $\hat{T}$  always lowers the critical speeds. If  $\hat{N} = 0$ , then  $\hat{\omega}_{C1}$  shows an asymptotic behaviour towards the first nondimensional natural frequency of a slender beam (dotted line in Fig. 14:  $\sqrt{\hat{\omega}_{C1}} = 4.730$  [24]), since increasing  $\alpha$  the Timoshenko model tends to the Euler–Bernoulli one. The case of traction ( $\hat{N} > 0$ ) produces a stiffening effect on the shaft, raising its critical speeds. The case of compression ( $\hat{N} < 0$ ) causes the opposite effect.

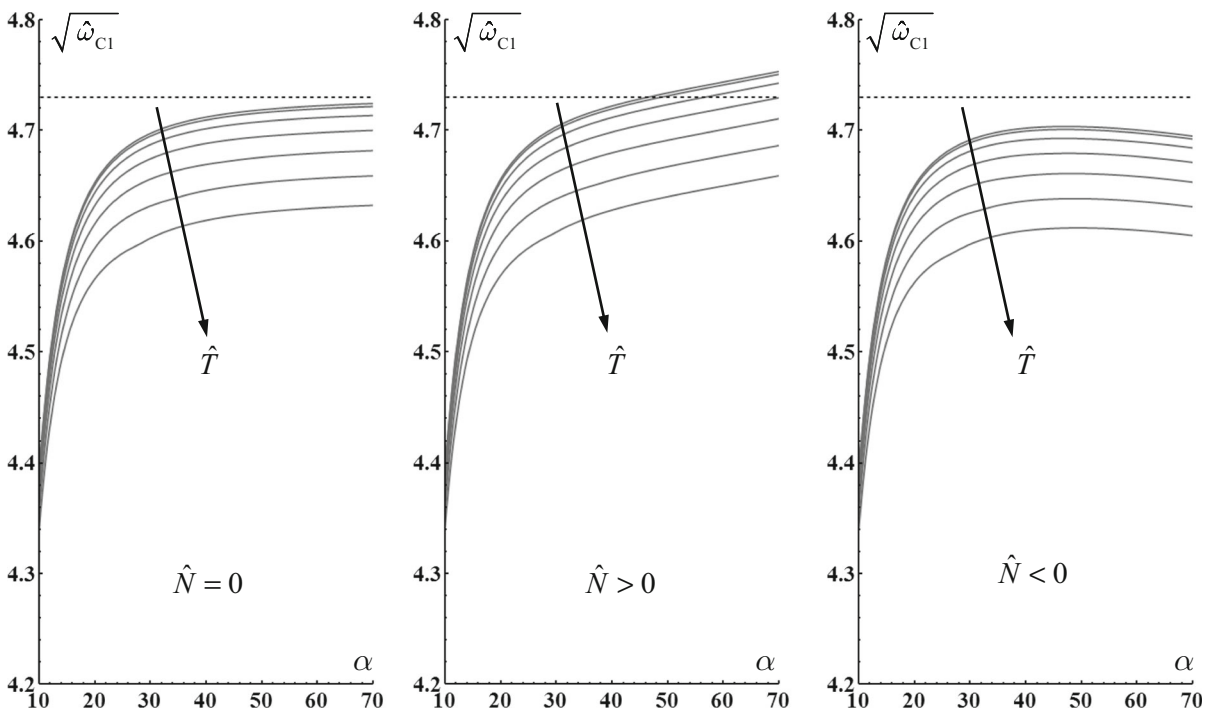


**Fig. 12** First forward critical speed  $\sqrt{\hat{\omega}_{C1}}$  as a function of  $\alpha$  for different values of  $\hat{T}$



### 6 Conclusions

A fast and easy to implement method has been proposed for the calculation of natural frequencies, modal shapes and critical speeds of a continuous rotating shaft, consisting of a homogeneous uniform Timoshenko straight beam, rotating at constant angular speed about its longitudinal axis and simultaneously subjected to axial end thrust and twisting moment.

The equations of motion have been derived in both Newtonian and Lagrangian formulations, correcting and clarifying some discrepancies existing in the literature. Modal analysis of the rotating shaft has then been developed for both complex and real displacement variables, presenting novel contributions in clarifying the relations between the two formulations, the structure of the algebraic and differential operators involved and the bi-orthogonality properties of the eigenfunctions in a state-space representation. The effects of varying the model main governing parameters, identified in slenderness ratio, angular speed, axial end thrust and twisting moment, have been studied on natural frequencies, modal shapes and critical speeds of the rotating shaft.

New evidence of existence of the second spectrum in the Timoshenko beam theory has been presented, together with a novel definition for its identification, only possible if considering gyroscopic effects. It has been found that the link between companion frequencies belonging to the first and second spectra is given by a peculiar asymptotic behaviour at high rotating speed. Each non-zero horizontal asymptote in Campbell diagrams represents a link between two pairs of eigenvalues, one pair at lower frequencies, one pair at higher frequencies. The latter, at zero angular speed and in particular cases of boundary conditions in which the characteristic equation factorizes (as in the case of simply supported ends), can be identified with the Timoshenko second spectrum. However, when considering a rotating shaft, as  $\omega \rightarrow \infty$  the existence of non-zero horizontal asymptotes for any boundary conditions suggests a new way for defining and identifying the natural frequencies of the Timoshenko first and second spectra. All first spectrum backward eigenfrequencies tend to 0; all second spectrum forward eigenfrequencies tend to infinity, while the absolute value of each first spectrum forward eigenfrequency converges to the backward companion one belonging to the second spectrum. As a result, it can be

stated that the whole second spectrum gives no contribution to the forward critical speeds. In parallel, the role of the so-called cut-off frequencies has been investigated, extending their definition to include the effects of gyroscopic moments and external loads.

The results of this study constitute the basis for further developments, including comparison with finite element models and rotor stability analysis under combined loads.

#### Compliance with ethical standards

**Conflict of interest** The authors declare that they have no conflict of interest.

### Appendix A. Kinetic energy density of the rotating shaft

A cross-section of infinitesimal length  $dx$  is considered, as represented in Fig. 13 with two coordinate systems, inertial  $(x, y, z)$  and floating  $(x', y', z')$ .

The velocity of the center of gravity ( $\mathbf{o}'$ ) of the cross-section is given by:

$$\mathbf{o}' = \mathbf{o} + \mathbf{s}, \quad \mathbf{q}' = \dot{\mathbf{s}} = \{\dot{u}, \dot{v}, \dot{w}\}^T \tag{A.1}$$

The absolute angular velocity of the cross-section  $\boldsymbol{\omega}$ , represented in the floating coordinate system, is the sum of a component  $\boldsymbol{\omega}_0$  given by the rotating angular speed of the shaft, plus a relative component  $\boldsymbol{\omega}_r$ , according to:

$$\boldsymbol{\omega} = \boldsymbol{\omega}_0 + \boldsymbol{\omega}_r, \quad \boldsymbol{\omega}_0 = \{\omega, 0, 0\}^T, \quad \tilde{\boldsymbol{\omega}}_r = \mathbf{R}^T \dot{\mathbf{R}} \tag{A.2}$$

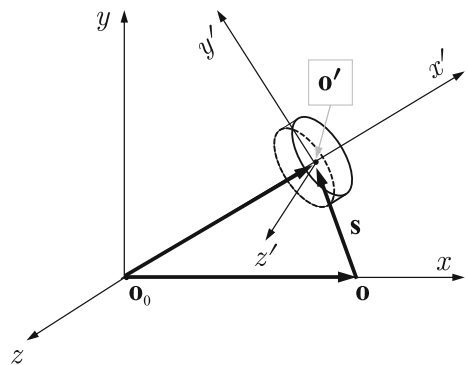


**Fig. 13** Reference systems (fixed and floating) for a cross-section of infinitesimal length  $dx$

where  $\boldsymbol{\omega}_r$  is written in skew-symmetric matrix form and  $\mathbf{R}$  is its associate rotation matrix. Since the first-order approximation of  $\mathbf{R}$  would lead to an incomplete expression of the kinetic energy (lacking of gyroscopic terms), a second-order approximation for small rotations is required. Therefore, the first-order approximation  $\mathbf{R}^{(1)}$  is expanded by addition of (small) second-order terms, say  $\varepsilon$ :

$$\mathbf{R}^{(1)} = \begin{bmatrix} 1 & -\vartheta_z & \vartheta_y \\ \vartheta_z & 1 & -\vartheta_x \\ -\vartheta_y & \vartheta_x & 1 \end{bmatrix} \Rightarrow \mathbf{R}^{(2)} = \begin{bmatrix} 1 - \varepsilon_{11} & -\vartheta_z + \varepsilon_{12} & \vartheta_y + \varepsilon_{13} \\ \vartheta_z + \varepsilon_{21} & 1 - \varepsilon_{22} & -\vartheta_x + \varepsilon_{23} \\ -\vartheta_y + \varepsilon_{31} & \vartheta_x + \varepsilon_{32} & 1 - \varepsilon_{33} \end{bmatrix} \tag{A.3}$$

As an alternative method to Taylor expansions of trigonometric terms due to selected (arbitrary) sequences of basic rotations (leading to non-univocal results, as discussed in [2]), here the  $\varepsilon$  terms are simply determined by requiring that: (1) the second-order approximation  $\mathbf{R}^{(2)}$  must respect the properties of a rotation matrix; (2) among all possible choices, the selected  $\mathbf{R}^{(2)}$  is the closest to  $\mathbf{R}^{(1)}$  (and therefore it is univocally determined). Imposing unit norm to all the columns of  $\mathbf{R}^{(2)}$  in Eq. (A.3), and neglecting all terms of order higher than two, yields:

$$\begin{aligned} \varepsilon_{11} &= \frac{1}{2}(\vartheta_y^2 + \vartheta_z^2), & \varepsilon_{22} &= \frac{1}{2}(\vartheta_x^2 + \vartheta_z^2), \\ \varepsilon_{33} &= \frac{1}{2}(\vartheta_x^2 + \vartheta_y^2) \end{aligned} \tag{A.4}$$

Introducing the expressions given by Eq. (A.4) into  $\mathbf{R}^{(2)}$ , then imposing the linear independency of all its columns, and neglecting again all terms of order higher than two, three further equations are written in the unknowns  $\varepsilon_{hk}$ , admitting an infinite set of solutions. For satisfying the request of minimal variations with respect to  $\mathbf{R}^{(1)}$ , equal values  $\varepsilon_{hk} = \varepsilon_{kh}$  are selected, yielding:

$$\begin{aligned} \varepsilon_{21} = \varepsilon_{12} &= \frac{1}{2}\vartheta_x\vartheta_y, & \varepsilon_{31} = \varepsilon_{13} &= \frac{1}{2}\vartheta_x\vartheta_z, \\ \varepsilon_{32} = \varepsilon_{23} &= \frac{1}{2}\vartheta_y\vartheta_z \end{aligned} \tag{A.5}$$

Hence the resulting second-order rotation matrix  $\mathbf{R}^{(2)}$  takes the form:

$$\mathbf{R} = \begin{bmatrix} 1 - \frac{1}{2}(\vartheta_y^2 + \vartheta_z^2) & -\vartheta_z + \frac{1}{2}\vartheta_x\vartheta_y & \vartheta_y + \frac{1}{2}\vartheta_x\vartheta_z \\ \vartheta_z + \frac{1}{2}\vartheta_x\vartheta_y & 1 - \frac{1}{2}(\vartheta_x^2 + \vartheta_z^2) & -\vartheta_x + \frac{1}{2}\vartheta_y\vartheta_z \\ -\vartheta_y + \frac{1}{2}\vartheta_x\vartheta_z & \vartheta_x + \frac{1}{2}\vartheta_y\vartheta_z & 1 - \frac{1}{2}(\vartheta_x^2 + \vartheta_y^2) \end{bmatrix} \tag{A.6}$$

Recalling Eqs. (A.1) and (A.2), the kinetic energy density  $\mathcal{T}$  of a cross-section of infinitesimal length  $dx$

can then be written as:

$$\mathcal{T} = \frac{1}{2}\rho (A \dot{\mathbf{s}}^T \dot{\mathbf{s}} + \boldsymbol{\omega}^T \mathbf{J} \boldsymbol{\omega}) \tag{A.7}$$

where  $\mathbf{J}$  is the cross-section tensor of inertia, consisting of a constant diagonal matrix with elements  $J_{11} = 2J$  and  $J_{22} = J_{33} = J$ . Developing the calculations, and truncating the result to second-order terms, yields the approximate expression of the kinetic energy density as reported in Eq. (7).

### Appendix B. Decoupling the equations of motion

The two fourth-order equations in the real variables  $v$  and  $w$ , Eq. (20), are decoupled into a single eighth-order equation in a real variable, say  $v$ . Laplace transforming with respect to time and adopting the following compact notation:

$$F_v = v^{\text{II}} - \frac{\sigma s^2}{\alpha^2} v, \quad F_w = w^{\text{II}} - \frac{\sigma s^2}{\alpha^2} w \tag{B.1}$$

Equations (20) are rewritten in the form:

$$\begin{cases} F_v^{\text{II}} + \hat{T} F_w^{\text{I}} - \hat{N} \alpha^2 \psi v^{\text{II}} + \psi s^2 v - \frac{s^2}{\alpha^2} F_v - 2\hat{\omega} \frac{s}{\alpha^2} F_w = 0 \\ F_w^{\text{II}} - \hat{T} F_v^{\text{I}} - \hat{N} \alpha^2 \psi w^{\text{II}} + \psi s^2 w - \frac{s^2}{\alpha^2} F_w + 2\hat{\omega} \frac{s}{\alpha^2} F_v = 0 \end{cases} \tag{B.2}$$

in which the  $v$ - and  $w$ -dependent terms can be rearranged as:



$$\begin{cases} F_w^I = 2\frac{\hat{\omega}}{\hat{T}}\frac{s}{\alpha^2}F_w + A_v \\ F_w^{II} = \hat{N}\alpha^2\psi w^{II} - \psi s^2w + \frac{s^2}{\alpha^2}F_w + B_v \\ A_v = \frac{1}{\hat{T}}\left(-F_v^{II} + \hat{N}\alpha^2\psi v^{II} - \psi s^2v + \frac{s^2}{\alpha^2}F_v\right) \\ B_v = \hat{T}F_v^I - 2\hat{\omega}\frac{s}{\alpha^2}F_v \end{cases} \tag{B.3}$$

Taking the first derivative with respect to  $\zeta$  of the first of Eq. (B.2):

$$\hat{T}F_w^{II} - 2\hat{\omega}\frac{s}{\alpha^2}F_w^I + C_v = 0, \quad C_v = -\hat{T}A_v^I \tag{B.4}$$

and introducing Eq. (B.3) yields  $w^{II}$  as a function of  $w$  and  $v$ :

$$\begin{aligned} w^{II} &= -\frac{1}{\beta_2}(\beta_1w + D_v), \\ D_v &= C_v + \hat{T}B_v - 2\hat{\omega}\frac{s}{\alpha^2}A_v, \\ \begin{cases} \beta_1 &= -\hat{T}\psi s^2 - \hat{T}\sigma\frac{s^4}{\alpha^4} + 4\sigma\frac{\hat{\omega}^2s^4}{\hat{T}\alpha^6} \\ \beta_2 &= \hat{T}\hat{N}\alpha^2\psi + \hat{T}\frac{s^2}{\alpha^2} - 4\frac{\hat{\omega}^2s^2}{\hat{T}\alpha^4} \end{cases} \end{aligned} \tag{B.5}$$

Recalling the definition of  $F_w$  in Eq. (B.1), then Eq. (B.5) give immediately:

$$F_w = -\beta_3w + E_v, \quad E_v = -\frac{D_v}{\beta_2}, \quad \beta_3 = \frac{\sigma s^2}{\alpha^2} + \frac{\beta_1}{\beta_2} \tag{B.6}$$

Taking the second derivative with respect to  $\zeta$  of Eq. (B.6):

$$F_w^{II} = E_v^{II} - \beta_3w^{II} \tag{B.7}$$

and introducing the expressions of  $F_w$  and of its second derivative given by Eqs. (B.3) and (B.5), as well as that of  $w^{II}$  given by Eq. (B.6), yields  $w$  as a function of  $v$ :

$$\begin{aligned} w &= \frac{G_v}{\beta_4}, \\ G_v &= B_v - \frac{1}{\beta_2}(\hat{N}\alpha^2\psi + \beta_3)D_v - E_v^{II} + \frac{s^2}{\alpha^2}E_v, \\ \beta_4 &= \hat{N}\alpha^2\psi\frac{\beta_1}{\beta_2} + \psi s^2 + \left(\frac{s^2}{\alpha^2} + \frac{\beta_1}{\beta_2}\right)\beta_3 \end{aligned} \tag{B.8}$$

Finally, the  $w$ -independent expressions of  $F_w$  and of its first derivative, obtained from Eqs. (B.6) and (B.8):

$$F_w = E_v - \frac{\beta_3}{\beta_4}G_v, \quad F_w^I = E_v^I - \frac{\beta_3}{\beta_4}G_v^I \tag{B.9}$$

are introduced in the first of Eq. (B.2) yielding an eighth-order equation in the real variable  $v$ :

$$\begin{aligned} F_v^{II} + \hat{T}\left(E_v^I - \frac{\beta_3}{\beta_4}G_v^I\right) - \hat{N}\alpha^2\psi v^{II} + \psi s^2v - \frac{s^2}{\alpha^2}F_v \\ - 2\hat{\omega}\frac{s^2}{\alpha^2}\left(E_v - \frac{\beta_3}{\beta_4}G_v\right) = 0 \end{aligned} \tag{B.10}$$

After substituting the expressions of  $F_v$ ,  $E_v$  and  $G_v$ , the resulting coefficients are:

$$\begin{aligned} q_8 &= 1, \quad q_7 = 0, \\ q_6 &= -\frac{2(1+\sigma)}{\alpha^2}s^2 + \hat{T}^2 - 2\hat{N}\alpha^2\psi, \\ q_5 &= -\frac{4\hat{T}\hat{\omega}}{\alpha^2}s, \\ q_4 &= \frac{1+\sigma(4+\sigma)}{\alpha^4}s^4 + [2\psi[1+\hat{N}(1+\sigma)] \\ &\quad - \frac{2\sigma\hat{T}^2}{\alpha^2} + \frac{4\hat{\omega}^2}{\alpha^4}]s^2 + \hat{N}^2\alpha^4\psi^2, \\ q_3 &= \frac{8\sigma\hat{T}\hat{\omega}}{\alpha^4}s^3, \quad q_2 = -\frac{2\sigma(1+\sigma)}{\alpha^6}s^6 \\ &\quad + \left[\frac{\sigma^2\hat{T}^2}{\alpha^4} - \frac{2\psi[1+\sigma(1+\hat{N})]}{\alpha^2} - \frac{8\sigma\hat{\omega}^2}{\alpha^6}\right]s^4 \\ &\quad - 2\hat{N}\alpha^2\psi^2s^2, \\ q_1 &= -\frac{4\sigma^2\hat{T}\hat{\omega}}{\alpha^6}s^5, \\ q_0 &= \frac{\sigma^2}{\alpha^8}s^8 + \left(\frac{2\sigma\psi}{\alpha^4} + \frac{4\sigma^2\hat{\omega}^2}{\alpha^8}\right)s^6 + \psi^2s^4 \end{aligned} \tag{B.11}$$

Applying the inverse Laplace transform back to time domain yields the decoupled eighth-order (with respect to both  $x$  and  $t$ ) partial differential equation of motion in the real variable  $v$ .

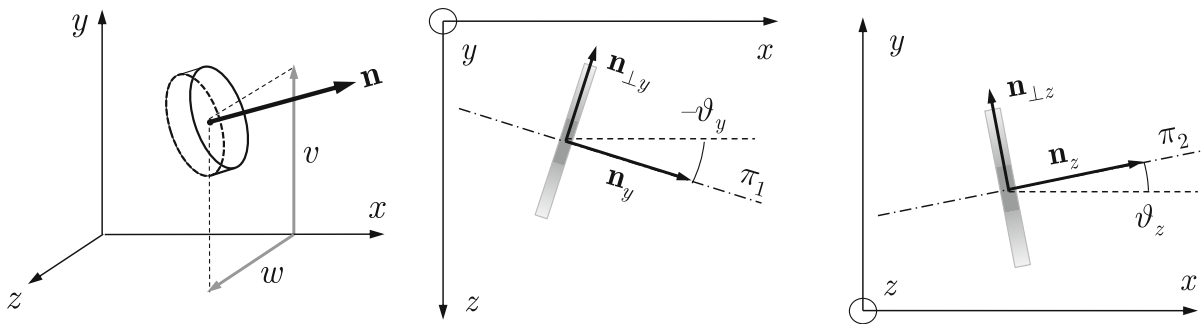


**Fig. 14** Schematic of a cross-section of the shaft in a generic position

**Appendix C. Representation of angular displacements**

The instantaneous position of a cross-section of the shaft can be represented in terms of displacement of its center ( $v, w$ ) and of a versor  $\mathbf{n}$  orthogonal to its surface (planar by assumption), as shown in Fig. 14 (left).

The projections of  $\mathbf{n}$  on the  $x$ - $y$  and  $x$ - $z$  orthogonal planes (say  $\mathbf{n}_z$  and  $\mathbf{n}_y$ , respectively) define two other planes, as represented in Fig. 14 (right), where  $\pi_1$  is parallel to  $\mathbf{n}_y$  and perpendicular to  $x$ - $z$ , while  $\pi_2$  is parallel to  $\mathbf{n}_z$  and perpendicular to  $x$ - $y$ . The projections of  $\mathbf{n}$ , along with the parametric representations of the  $\pi$  planes, can be expressed as functions of the angular displacements  $\vartheta_y$  and  $\vartheta_z$ :

$$\frac{\mathbf{n}_y}{\|\mathbf{n}_y\|} = \begin{Bmatrix} \cos \vartheta_y \\ 0 \\ -\sin \vartheta_y \end{Bmatrix}, \quad \mathbf{p}_{\pi_1} = \begin{Bmatrix} n_1 \cos \vartheta_y \\ h_1 \\ -n_1 \sin \vartheta_y \end{Bmatrix},$$

$$\frac{\mathbf{n}_z}{\|\mathbf{n}_z\|} = \begin{Bmatrix} \cos \vartheta_z \\ \sin \vartheta_z \\ 0 \end{Bmatrix}, \quad \mathbf{p}_{\pi_2} = \begin{Bmatrix} n_2 \cos \vartheta_z \\ n_2 \sin \vartheta_z \\ h_2 \end{Bmatrix} \tag{C.1}$$

The orthogonal directions with respect to the  $\pi$  planes are identified by:

$$\mathbf{n}_{\perp y} = \frac{\partial \mathbf{p}_{\pi_1}}{\partial h_1} \times \frac{\partial \mathbf{p}_{\pi_1}}{\partial n_1} = \begin{Bmatrix} -\sin \vartheta_y \\ 0 \\ -\cos \vartheta_y \end{Bmatrix},$$

$$\mathbf{n}_{\perp z} = \frac{\partial \mathbf{p}_{\pi_2}}{\partial h_2} \times \frac{\partial \mathbf{p}_{\pi_2}}{\partial n_2} = \begin{Bmatrix} -\sin \vartheta_z \\ \cos \vartheta_z \\ 0 \end{Bmatrix} \tag{C.2}$$

which give a definition of  $\mathbf{n}$  as a function of  $\vartheta_y$  and  $\vartheta_z$ :

$$\mathbf{n} = \frac{\mathbf{n}^+}{\|\mathbf{n}^+\|},$$

$$\mathbf{n}^+ = \mathbf{n}_{\perp y} \times \mathbf{n}_{\perp z} = \begin{Bmatrix} \cos \vartheta_y \cos \vartheta_z \\ \cos \vartheta_y \sin \vartheta_z \\ -\sin \vartheta_y \cos \vartheta_z \end{Bmatrix} \tag{C.3}$$

Equations (C.3) provide an unambiguous representation of the cross-section orientation in terms of angular displacements ( $\vartheta_y, \vartheta_z$ ), which in Sect. 5.3 has been adopted for improving the readability of plots.

**References**

1. Dimentberg FM (1961) Flexural vibrations of rotating shafts. Butterworth, London
2. Raffa FA, Vatta F (1999) Gyroscopic effects analysis in the lagrangian formulation of rotating beams. Meccanica 34:357–366
3. Raffa FA, Vatta F (2001) Equations of motion of an asymmetric Timoshenko shaft. Meccanica 36:201–211
4. Filipich CP, Rosales MB (1990) Free flexural-torsional vibrations of a uniform spinning beam. J Sound Vib 141(3):375–387
5. Greenhill AG (1883) On the strength of shafting when exposed both to torsion and to end thrust. Proc Inst Mech Eng Lond 6:182–209
6. Southwell RV, Gough BS (1921) On the stability of rotating shaft, subjected simultaneously to end thrust and twist. Br Assoc Adv Sci 345:38–59
7. Colomb M, Rosenberg RM (1951) Critical speeds of uniform shafts under axial torque. In: Proceedings of First U.S. National Congress of applied mechanics, New York, USA, pp 103–110
8. Eshleman RL, Eubanks RA (1969) On the critical speeds of a continuous rotor. Trans Am Soc Mech Eng, J Eng Ind 91(4):1180–1188
9. Yim KB, Noah ST, Vance JM (1986) Effect of tangential torque on the dynamics of flexible rotors. Trans Am Soc Mech Eng, J Appl Mech 53:711–718

10. Choi SH, Pierre C, Ulsoy AG (1992) Consistent modeling of rotating Timoshenko shafts subject to axial loads. *ASME J Vib Acoust* 114:249–259
11. Willems N, Holzer S (1967) Critical speeds of rotating shafts subjected to axial loading and tangential torsion. *Trans Am Soc Mech Eng, J Eng Ind* 89:259–264
12. Dubigeon S, Michon JC (1975) Gyroscopic behaviour of stressed rotating shafts. *J Sound Vib* 42(3):281–293
13. Lee CW, Katz R, Ulsoy AG, Scott RA (1988) Modal analysis of a distributed parameter rotating shaft. *J Sound Vib* 122(1):119–130
14. Traill-Nash RW, Collar AR (1953) The effects of shear flexibility and rotatory inertia on the bending vibrations of beams. *Q J Mech Appl Math* 6(2):186–222
15. Levinson M, Cooke DW (1982) On the two frequency spectra of Timoshenko beams. *J Sound Vib* 84(3):319–326
16. Stephen NG (2006) The second spectrum of Timoshenko beam theory—further assessment. *J Sound Vib* 292:372–389
17. Stephen NG, Puchegger S (2006) On the valid frequency range of the Timoshenko beam theory. *J Sound Vib* 297:1082–1087
18. Diaz-de-Anda A, Flores J, Gutierrez L, Mendez-Sanchez RA, Monsivais G, Morales A (2012) Experimental study of the Timoshenko beam theory predictions. *J Sound Vib* 331:5732–5744
19. Manevich AI (2015) Dynamic of Timoshenko beam on linear and nonlinear foundation: phase relations, significance of the second spectrum, stability. *J Sound Vib* 344:209–220
20. De Felice A, Sorrentino S (2017) Insights into the gyroscopic behaviour of axially and torsionally loaded rotating shafts. In: *Proceedings of 24th international conference on sound and vibration (ICSV24)*, London United Kingdom: paper 879
21. De Felice A, Sorrentino S (2018) The second spectrum in Timoshenko beam theory: a new approach for its identification. In: *Proceedings of 25th international conference on sound and vibration (ICSV25)*, Hiroshima, Japan: paper 780
22. Raffa FA, Vatta F (2007) Dynamic instability of axially loaded shafts in the Mathieu map. *Meccanica* 42:347–553
23. Cowper GR (1966) The shear coefficient in Timoshenko's beam theory. *J Appl Mech* 33(2):335–340
24. Blevins RD (1979) *Formulas for natural frequency and mode shape*. Van Nostrand, New York

**Publisher's Note** Springer Nature remains neutral with regard to jurisdictional claims in published maps and institutional affiliations.